# Interblock Transmissibility Calculation Analysis for Petroleum Reservoir Simulation

Jonas Cordazzo, jonas@sinmec.ufsc.br
Clovis Raimundo Maliska, maliska@sinmec.ufsc.br
Antonio Fabio Carvalho da Silva, fabio@emc.ufsc.br

*Computational Fluid Dynamics Laboratory – SINMEC*
*www.sinmec.ufsc.br*
*Department of Mechanical Engineering, Federal University of Santa Catarina – UFSC*
*88.100.000, Florianopolis, Santa Catarina, Brazil*

**Abstract:** Field-scale reservoir simulations are usually carried out using corner-point grids (Ponting, 1989) with a 5-point stencil for the sake of simplicity of the whole numerical scheme. Although the use of these grids permits a good representation of reservoir geological features and reservoir description, the use of 5-point scheme yields wrong results, since fluxes through interfaces are calculated using only two grid points. It is well known that the use of two grid points for the flux calculation only gives accurate results if the grid is locally orthogonal. In this paper, this key issue is addressed through a study of several different ways of calculating the transmissibility using two grid points. Due to the physical similarity of the equations, heat conduction problems with analytical solution are used for comparing the results for the transmissibility between grid blocks. Following, it is proposed an EbFVM-Element-based Finite Volume Method using mixed triangular and quadrilateral elements for the simulation of multi-phase flows in porous media. The proposed method retains the geometric flexibility of the finite-element procedure and derives the governing discrete algebraic equations by using a conservation balance applied to discrete control volumes distributed throughout the domain. The method resembles the one used in fluid mechanics and heat transfer calculations, allowing the evaluation of the mobility in eight integration points when a quadrilateral element is used. Since the grid can be unstructured and arbitrary, local grid refinement for near-well resolution can be achieved in a simple and consistent manner. Transmissibility terms are embodied in the coefficients and are not individually identified. An analysis of a skew method used to calculate the mobility is also done.

## 1. Introduction

In this paper we discuss important aspects related to the grids used for petroleum reservoir simulation. Initially, the transmissibility is presented in the framework of boundary-fitted grids in order to study the two-point approximation approach. It will be possible to clearly identify the terms that are neglected in the flux calculation and how they affect the results. The traditional methods in petroleum engineering, as reported by Sammon (2000), employ, in general, two-point flux approximation scheme in order to reduce the computational cost.

In addition, this paper presents several examples of transmissibility calculation using a commercial simulator, where the results, in some cases, agree with the equations presented here, and in others, they do not. The differences are then plotted for different geometries.

Finally, the basic ideas of a new numerical scheme for reservoir simulation are presented. They are based on the EbFVM (Element based Finite Volume Method), and it can mix triangular and quadrilateral elements. In this method the transmissibility terms are embodied in the coefficients and are not individually identified. It results, for a 2D situation, in a nine-point scheme for both the pressure and the mobility.

## 2. Transmissibility definition

The focus of this paper is to analyze the conductance that appears in mass transfer problems in petroleum engineering. In other words, we want to study the water, oil and gas mass flow in a porous media. This special conductance, in this problem, is called *transmissibility*, and it involves intrinsic and relative permeabilities, fluid viscosity, the formation volume factor, and geometric parameters. Our interest in this paper is to analyze only the effects of the grid geometry on the transmissibility, i.e., we consider known all physical parameters. Therefore, it will be assumed a media with homogeneous mobility. No phases subscript will be used here, and a two dimensional problem is presented for simplicity with no loss of generality. So, the equation for one of the components in a multiphase flow is given by

$$\nabla \cdot (\lambda \nabla P) = \frac{\partial}{\partial t}\left(\varphi \frac{S}{B}\right) + \quad \bar{q} \tag{1}$$

where $P$ is the pressure, $\lambda$ is the mobility, $\phi$ is the porosity, $S$ is the saturation, $B$ is the formation volume factor and $\bar{q}$ is the flow rate per unit of reservoir volume, at reservoir conditions.

As we can see, Eq. (1) is in the vector form and can be written for any coordinate systems (Maliska, 1995). For our two dimensional problem, consider the following coordinate transformation $\xi = \xi(x, y)$, $\eta = \eta(x, y)$ and $\tau = t$.

Written in the new $(\xi, \eta)$ system, Eq. (1) is given by

$$\frac{1}{J}\frac{\partial}{\partial t}\left(\phi \frac{S}{B}\right) + \frac{\bar{q}}{J} = \frac{\partial}{\partial \xi}\left(D_1 \frac{\partial P}{\partial \xi} + D_2 \frac{\partial P}{\partial \eta}\right) + \frac{\partial}{\partial \eta}\left(D_3 \frac{\partial P}{\partial \xi} + D_4 \frac{\partial P}{\partial \eta}\right) \tag{2}$$

For a constant $\lambda$, we have

$$D_1 = \Gamma\left(x_\eta{}^2 + y_\eta{}^2\right) J \tag{3}$$

$$D_2 = -\Gamma\left(x_\xi x_\eta + y_\xi y_\eta\right) J \tag{4}$$

$$D_3 = -\Gamma\left(x_\xi x_\eta + y_\xi y_\eta\right) J \tag{5}$$

$$D_4 = \Gamma\left(x_\xi{}^2 + y_\xi{}^2\right) J \tag{6}$$

where $J$ is the Jacobian of the transformation and

$$\Gamma = \lambda = \frac{k \cdot k_r}{B\mu} \tag{7}$$

where $\lambda$ is the mobility, $k$ and $k_r$ are the intrinsic and relative permeabilities, respectively, $\mu$ is the fluid viscosity, and $B$ *is* the formation volume factor.

We can define the metric tensor $\underset{\sim}{g}$ as

$$\underset{\sim}{g} = \begin{bmatrix} g_{11} & g_{12} \\ g_{21} & g_{22} \end{bmatrix} \tag{8}$$

where the components are

$$g_{22} = \alpha = x_\eta^{\,2} + y_\eta^{\,2} \tag{9}$$

$$g_{11} = \gamma = x_\xi^{\,2} + y_\xi^{\,2} \tag{10}$$

and

$$g_{12} = g_{21} = \beta = x_\xi x_\eta + y_\xi y_\eta \tag{11}$$

It is important to recognize that in Eq. (2) the terms

$$D_1 \frac{\partial P}{\partial \xi} + D_2 \frac{\partial P}{\partial \eta} \qquad \text{and} \qquad D_3 \frac{\partial P}{\partial \xi} + D_4 \frac{\partial P}{\partial \eta}$$

represent, respectively, the fluxes through a $\xi$=constant and $\eta$=constant surfaces, as shown in Fig. 1.

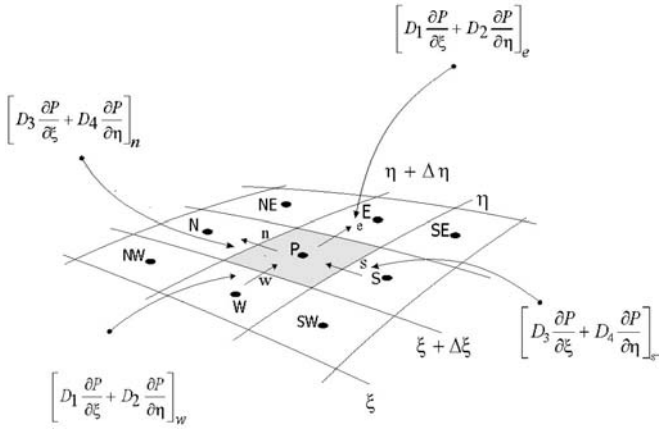


**Fig. 1- Control volume and surface fluxes**

These terms appear when Eq. (2) is integrated in the control volume and represents, therefore, the fluxes at the control volume surfaces. These are the fluxes that should be used for the transmissibility determination in its exact form. The east (*e*) surface flux, for example, is given by

$$f_e = D_1 \frac{\partial P}{\partial \xi} + D_2 \frac{\partial P}{\partial \eta} \tag{12}$$

where $D_1 = \Gamma\alpha J$ and $D_2 = -\Gamma\beta J$.

The first important observation is that in non-orthogonal grids the flux evaluation will be always in error if the cross-derivative term $\partial P / \partial \eta$ is set to zero in Eq. (12).

If $\partial P / \partial \eta$ is not set to zero, the algorithm will require, for a non-orthogonal grid, 9 points for 2D and 19 points for 3D. This term disappears when the grid is orthogonal, since, in this case, $\beta$, defined by Eq. (11) is zero.

The flux in east surface is, therefore, calculated in the exact way as

$$f_e = \Gamma\alpha J \frac{\partial P}{\partial \xi} - \Gamma\beta J \frac{\partial P}{\partial \eta} \tag{13}$$

Using Fig. 2 one can show some geometric relationships (Maliska, 1995) that will be used in the next equations. They are

$$dL_\xi = \sqrt{\gamma}\,\Delta\xi \tag{14}$$

and

$$dL_\eta = \sqrt{\alpha}\,\Delta\eta \tag{15}$$

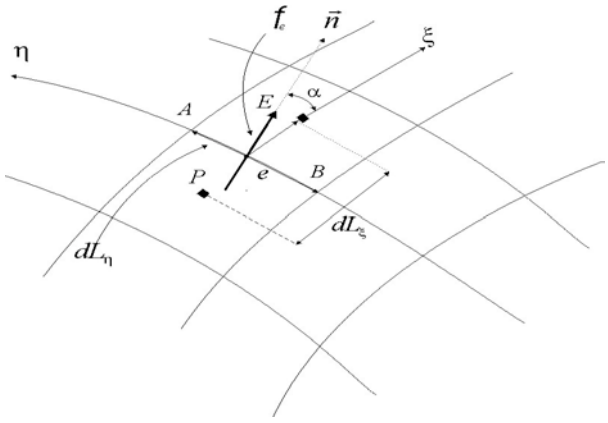


**Fig. 2- Some important geometrical relationships**

Eq. (13) can be rewritten as

$$f_e = \Gamma\sqrt{\alpha}\left(J\sqrt{\alpha}\frac{\partial P}{\partial \xi} - J\frac{\beta}{\sqrt{\alpha}}\frac{\partial P}{\partial \eta}\right) \tag{16}$$

where the term $\sqrt{\alpha}$ was put outside of the brackets in order to obtain the flux area. We can notice that the distance $\overline{AB}$, defined in Fig. 2, is $\sqrt{\alpha} = \sqrt{g_{22}}$, which is the flux area and, therefore, it should takes part in the transmissibility expressions.

It is easily demonstrated that the term in brackets in Eq. (16) is, exactly, $\partial P / \partial \vec{n}$ where $\vec{n}$ is the normal vector to the area $\sqrt{\alpha}$. Rewriting Eq. (16), one obtains

$$f_e = \Gamma \sqrt{\alpha} \; . \frac{\Delta P}{\Delta \vec{n}} \tag{17}$$

Using Eq. (17) we can now define the transmissibility as

$$T = \frac{\Gamma \sqrt{\alpha}}{\Delta n} \tag{18}$$

where $\Delta n$ is the distance between two grid points lying over the normal direction, as shown in Fig. 3. It is clear that other points than P and E will be needed for evaluating pressures at points 1 and 2.

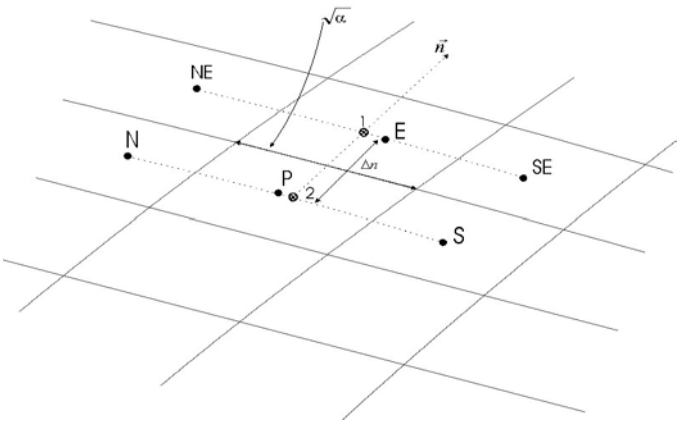


**Fig. 3- Evaluation of pressure gradient in the normal direction**

Therefore, the scheme that calculates the flux by

$$f_e = \frac{\Gamma \sqrt{\alpha}}{\Delta n} (P_1 - P_2) \tag{19}$$

is exact, except for truncation errors due to the numerical approximation. In other words, with the pressure in the normal direction the transmissibility

$$T = \frac{\Gamma \sqrt{\alpha}}{\Delta n} \tag{20}$$

is exact . The scheme, however, involves 9 points.

Interpolating points on the normal direction is not a practical process, and it is desirable to use only two grid points. Returning to Eq. (16),

$$f_e = \Gamma \sqrt{\alpha} \left( J \sqrt{\alpha} \frac{\partial P}{\partial \xi} - J \frac{\beta}{\sqrt{\alpha}} \frac{\partial P}{\partial \eta} \right) \tag{21}$$

and keeping in mind that $\sqrt{\alpha}$ is the flux area and after some algebraic manipulations, Eq. (21) yields

$$f_e = \Gamma \sqrt{\alpha} \left( J \sqrt{\alpha} \frac{\sqrt{\gamma}}{\sqrt{\gamma}} \frac{\partial P}{\partial \xi} - J \frac{\beta}{\sqrt{\alpha}} \frac{\partial P}{\partial \eta} \right) \tag{22}$$

Substituting the equations (14) and (15) in (22), one obtains

$$f_e = \Gamma \sqrt{\alpha} \left( J \sqrt{\alpha} \sqrt{\gamma} \frac{\Delta P}{\Delta L_\eta} \right) - \Gamma \sqrt{\alpha} \left( J \beta \frac{\Delta P}{\Delta L_\eta} \right) \tag{23}$$

It is easy to show that (Maliska, 2001)

$$\sqrt{\alpha} \sqrt{\gamma} J = \frac{1}{\cos \alpha}$$

and

$$\beta J = J \sqrt{\gamma} \sqrt{\alpha} \cos \theta \tag{24}$$

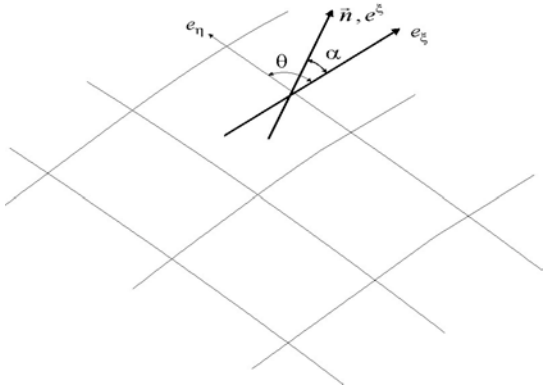


**Fig. 4 – Relationship between $\alpha$ and $\theta$ angles**

The $\alpha$ angle in Fig. 4 should not be confused with the component of metric tensor $g_{11}$. Using Eq. (24), Eq. (23), yields

$$f_e = \Gamma \sqrt{\alpha} \left( J \sqrt{\alpha} \sqrt{\gamma} \frac{\Delta P}{\Delta L_\xi} - J \sqrt{\alpha} \sqrt{\gamma} \cos\theta \frac{\Delta P}{\Delta L_\eta} \right) \tag{25}$$

or

$$f_e = \Gamma \sqrt{\alpha} \underbrace{J \sqrt{\alpha} \sqrt{\gamma}}_{\frac{1}{\cos\alpha}} \left( \frac{\Delta P}{\Delta L_\xi} - \frac{\Delta P}{\Delta L_\eta} \cos\theta \right) \tag{26}$$

Inspecting Fig. 4, and algebraically manipulating the $\theta$ and $\alpha$ angles, we can see that Eq. (26) yields

$$f_e = \Gamma \sqrt{\alpha} \left( \frac{\Delta P}{\Delta L_\xi} \frac{1}{\cos\alpha} + \frac{\Delta P}{\Delta L_\eta} \frac{sen\alpha}{\cos\alpha} \right) \tag{27}$$

Using Eq. (27), we can analyze the transmissibility equations. With the help of Fig. 5, one can see that the

interface area ($A$) of element P has a relationship with flux normal area ($A_P$) by

$$\begin{aligned} \overline{AB} &= \sqrt{\alpha} = A \\ \overline{AC} &= A\cos\alpha = A_P \end{aligned} \tag{28}$$

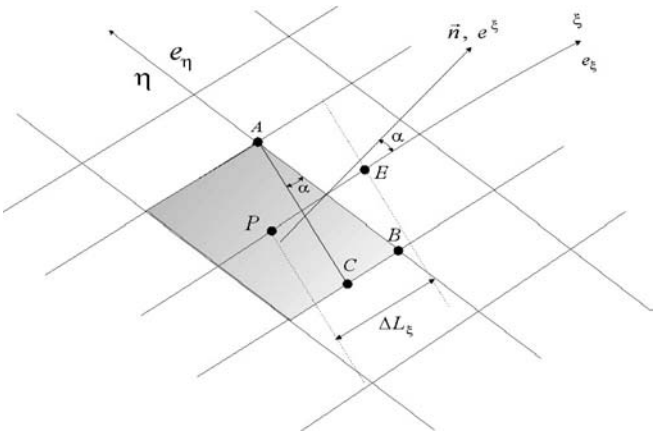


**Fig. 5 – Relationship between interface area and normal area**

Therefore, Eq. (27) can be written as

$$f_e = \frac{\Gamma A}{\cos\alpha}\left(\frac{\Delta P}{\Delta L_\xi} + \frac{\Delta P}{\Delta L_\eta} sen\alpha\right) \tag{29}$$

or

$$f_e = \frac{\Gamma A \cos\alpha}{\cos^2\alpha}\left(\frac{\Delta P}{\Delta L_\xi} + \frac{\Delta P}{\Delta L_\eta} sen\alpha\right) \tag{30}$$

or

$$f_e = \frac{\Gamma A_P}{\cos^2\alpha}\left(\frac{\Delta P}{\Delta L_\xi} + \frac{\Delta P}{\Delta L_\eta} sen\alpha\right) \tag{31}$$

Up to now no simplifications were made and the value of $f_e$ in Eq. (31) is exact.

To avoid nine point schemes (or 19 in 3D), we can neglect the term $(\Delta P / \Delta L_\eta) sen\alpha$. If $\alpha$ is small, this approximation may not be too serious. Note that since there are not absolute rules in engineering, neglecting this term depends on the quality of the solution one wants. If this simplification is reasonable, the flux can be calculated by

$$f_e = \underbrace{\frac{\Gamma A_P}{\Delta L_\xi \cos^2\alpha}}_{transmissibility}\left(P_E - P_P\right) \tag{32}$$

Obviously the flux calculated in this way is not correct because the term $\partial P / \partial \eta$ was neglected.

In the transmissibility definition given in Eq. (32), the area is normal to the length that appears in the denominator ($\Delta L_\xi$), as it should be. Eq. (29) could be written also as

$$f_e = \frac{\Gamma A}{\cos\alpha \Delta L_\xi}\left(P_E - P_P\right) \tag{33}$$

Eqs. (32) and (33) are identical, but is rearranged in order to appear the factor $\cos^2\alpha$.

Therefore, the transmissibility for a two-point approximation scheme for the flux is given by

$$T = \frac{\Gamma A_P}{\Delta L_\xi \cos^2\alpha} \tag{34}$$

The flux given by $f_e = T.(P_E - P_P)$ contains errors due to the simplification of $(\Delta P / \Delta L_\mu) sen\alpha = 0$.

Note that in two dimensional problems, for example, the transmissibility only appears explicitly in schemes that use 5 points to approximate the flux. In 9-point schemes, on the other hand, transmissibility terms are embodied in the coefficients and are not individually identified.

### 3. Transmissibility Approach in Reservoir Simulators

Most reservoir simulation models use two-point flux approximation schemes. The motivation for this choice is the reduction of computational effort. Heinemann & Brand (1989) presented the procedure more employed in simulators, and it is described below. The mass flux of a component between two adjacent grid-blocks *i and j* in the discrete solution of the transport equations is given by

$$Q_{ij} = \sum_{p=1}^{P} \left(\Lambda_p k\right)_{ij} \frac{A_{ij}}{h_{ij}} \left(\Phi_j - \Phi_i\right)_p \tag{35}$$

where $\Lambda_p$ is the mobility of phase $p$, $P$ is the number of phases; $k$ is the absolute permeability; $\Phi$ is the phase potential, $A_{ij}$ and $h_{ij}$ are, respectively, an area where the mass flows and an adequate length for the gradient determination in the surface. The procedure usually utilized to determine the last two geometric parameters will be present in chapter 3.1.

In Eq. (35), the terms independent of pressure and saturation can be grouped in the form

$$Q_{ij} = T_{ij} \sum_{p=1}^{P} \left(\Lambda_p\right)_{ij} \left(\Phi_j - \Phi_i\right)_p \tag{36}$$

where $T_{ij}$ is called transmissibility which is, therefore, defined as

$$T_{ij} = k_{ij} \frac{A_{ij}}{h_{ij}} \tag{37}$$

The inverse of the transmissibility is the resistivity given by

$$r = \frac{1}{T} \tag{38}$$

Transmissibility depends only on block geometry and permeability. When using conservative numerical methods, the integration of differential equations in the divergent form demands the calculation of the fluxes in the control volume interfaces. As the domain may be heterogeneous, sometimes with great differences in terms of permeability in adjacent grid-blocks, the definition of average properties in the interface can result in errors in the flux calculation. The most appropriate procedure to calculate transmissibility is to model it as the inverse of the resistance in each control volume. As already stated, for orthogonal grids with fully coincident interfaces this procedure leads to the exact flux determination. On the other hand, for non-orthogonal grids, grids with partial contact between the grid-blocks or with local refinement, the flux surfaces need to be defined. The Ohm's Law can be applied to calculate the total resistance, and in consequence the total transmissibility, for elements connected in series or in parallel because Eq. (35) is linear in the potential difference. For the case of a series connection, as shown in Fig. 6, we have

$$r_{12} = r_1 + r_2 = \frac{1}{T_1} + \frac{1}{T_2} \tag{39}$$

where $r_i$ is the inner-block $i$ flow resistance and $T_i$ is the transmissibility of block $i$. So, the total transmissibility between two grid-blocks 1 and 2 is given by

$$T_{12} = \frac{1}{r_{12}} = \frac{1}{\frac{1}{T_1} + \frac{1}{T_2}} = \frac{T_1 T_2}{T_1 + T_2} \tag{40}$$

where the transmissibility calculated in this way constitutes a harmonic averaging of the transmissibilities in blocks 1 and 2.

In this work, as shown earlier, we represent with only one subscript the transmissibilities determined by geometric and permeability parameters of one block only ($T_1$, for example). For the case where transmissibilities are calculated using two blocks properties, we represent it using two subscripts, like $T_{12}$, for example.

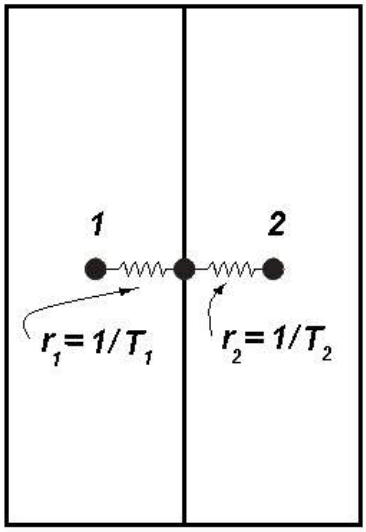


**Fig. 6 – Calculation of transmissibility using the analogy with electricity**

As there is the possibility of partial contact between two grid-blocks, as shown Fig. 7, the total transmissibility can be calculated as

$$T_{12} = \frac{A_c}{\frac{A_1}{T_1} + \frac{A_2}{T_2}} \tag{41}$$

where $A_c$ is the contact surface, $A_1$ and $A_2$ are the complete surface of each neighbor, and $T_1$ and $T_2$ are their inner transmissibilities. We can observe that in this case we chose to use the area $A_c$, the contact area, to calculate the transmissibilities of grid-blocks 1 and 2, which is an approximation that will not lead to the exact value, even with grid refinement. If the adjacent blocks are in fully contact the interface areas $A_1=A_2=A_c$, and Eq. (41) can be written as

$$T_{12} = \frac{A_c}{\frac{A_1}{T_1} + \frac{A_2}{T_2}} = \frac{A_c}{\frac{A_c}{T_1} + \frac{A_c}{T_2}} = \frac{1}{\frac{1}{T_1} + \frac{1}{T_2}} = \frac{T_1 T_2}{T_1 + T_2} \tag{42}$$

which is the Eq. (40) already shown.

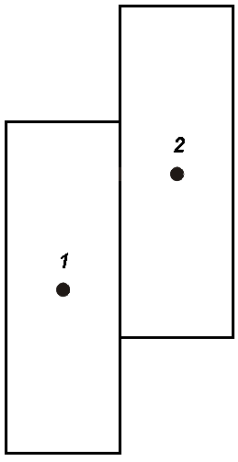


**Fig. 7 – Partial contact between two grid-blocks**

In the most general case, when $A_1 \neq A_2 \neq A_c$, as shown in Fig. 7, Eq. (41) results in

$$T_{12} = \frac{A_c}{\frac{A_1}{T_1} + \frac{A_2}{T_2}} = \frac{1}{\frac{A_1}{A_c T_1} + \frac{A_2}{A_c T_2}} = \frac{1}{\frac{1}{\frac{A_c}{A_1} T_1} + \frac{1}{\frac{A_c}{A_2} T_2}} \qquad (43)$$

which can be seen as being Eq. (40) weighted by the areas. The contact area divided by grid-block area appears as a multiplying factor for each transmissibility. If these areas are $A_1 \neq A_2 \neq A_c$ and locally non-orthogonal, as shown in Fig. 8, there is the need of not only a surface multiplier but also of some type of projection of the surface. In this case, again, the transmissibility will not tend to the exact value with grid refinement, what would be expected in any numerical solution. Thus, when non-orthogonal grids and/or grids with partial contact are used, the flux calculation can not be exactly calculated if only two grid points are used. The only exception for this rule happens when the problem is one dimensional, and in this case, as it is shown in next chapter, the transmissibility calculation with two grid-points is exact.

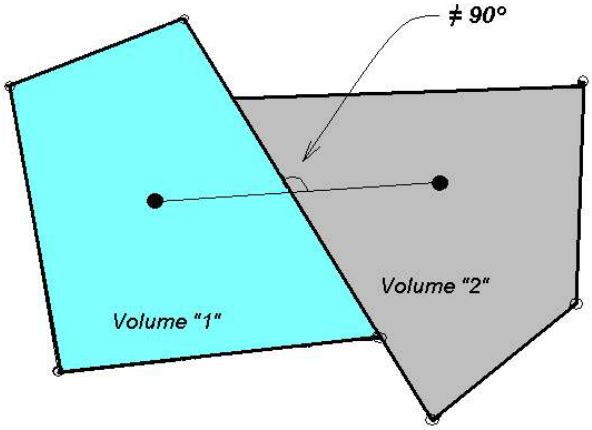


**Fig. 8 – Locally non-orthogonal grid-blocks (volumes)**

### 3.1 – Usual procedure for the determination of areas and lengths in the transmissibility calculation for 3D grids

The schemes for calculating the transmissibilities used by most reservoir simulators that use corner point grids will be considered in this section. A volume created in this way is defined by 8 corners. Such grids can be severely faulted and the corner point volumes near the faults, and elsewhere, can be distorted. Fig. 9 presents a cell built by corner definition.

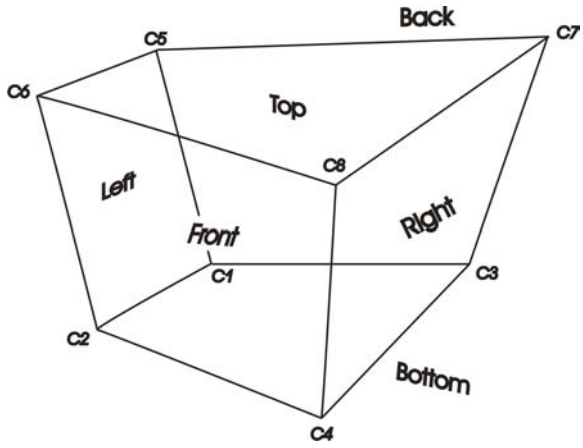


**Fig. 9 – Corner point grid (Sammon, 2000)**

Sammon (2000) presents the procedure used by most reservoir simulators; one of them being the software IMEX (Implicit Explicit Black Oil Simulator) by CMG (Computer Modelling Group Ltd.) (Salazar, 2002). Here we will present briefly the transmissibility calculation schemes for corner point grids. Assume that the cell in Fig. 9 contacts another cell through its front face. Then, the vector that is parallel to the vector that goes through the barycentre of the volume and frontal face is given by

$$\mathbf{v} = [\mathbf{C}2 - \mathbf{C}1 + \mathbf{C}4 - \mathbf{C}3 + \mathbf{C}6 - \mathbf{C}5 + \mathbf{C}8 - \mathbf{C}7] / 4 \qquad (44)$$

Notice that any vector **C**i is a vector that has its origin in the origin of the coordinate system, and its end in point Ci. In other words, **C**1 is a vector and C1 is the end point this vector, where the only typing difference is the bold letter. Therefore, in this case, the module of vector **v** is the length of the straight line that goes through the centre of the surface built using points C2, C4, C6 and C8 and goes through the centre of the surface created by points C1, C3, C5 and C7. Its unit vector is given by

$$\hat{\mathbf{v}} = \mathbf{v} / |\mathbf{v}| \qquad (45)$$

The contact area aligned with this centre-to-centre line is

$$A = \iint \langle \hat{\mathbf{v}}, d\mathbf{S}(\mathbf{P}) \rangle \qquad (46)$$

Calling the adjacent grid-blocks as "1" and "2", there are two vectors: $\mathbf{v}_1$ and $\mathbf{v}_2$, and two effective areas that need to be computed:

$$A_1 = \iint \langle \hat{\mathbf{v}}_1, d\mathbf{S}(\mathbf{P}) \rangle \quad \text{and} \quad A_2 = \iint \langle \hat{\mathbf{v}}_2, d\mathbf{S}(\mathbf{P}) \rangle \qquad (47)$$

Notice that there is the possibility of partial contact between these two blocks, and then the total transmissibility $T_{12}$ can be determined, as already stated, by

$$T_{12} = \frac{A_c}{\frac{A_1}{T_1} + \frac{A_2}{T_2}} \qquad (48)$$

where $A_c$ is the contact area, $A_1$ and $A_2$ are the effective areas, and $T_1$ and $T_2$ are transmissibilities given by

$$T_1 = \frac{k_1 A_1}{\frac{|\mathbf{v}_1|}{2}} \qquad \text{and} \qquad T_2 = \frac{k_2 A_2}{\frac{|\mathbf{v}_2|}{2}} \tag{49}$$

where $k_1$ and $k_2$ are the permeabilities of each volume. Note that Eq. (48) is the same equation present in Hegre *et al.* (1986).

For the case shown in Fig. 10, i.e. for a geometry where its volumes have full contact, and the centre-to-centre line of the volumes is orthogonal to the flux surface, the transmissibility of volume 1, for example, is given by

$$T_1 = \frac{k_1 \Delta z \Delta y}{\frac{\Delta x}{2}} \tag{50}$$

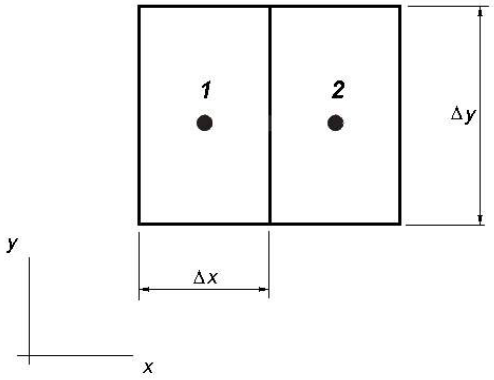


**Fig. 10 – Regular geometry blocks**

On the other hand, Fig. 11 presents a case where a volume is connected to other two volumes. This situation can appear in local refinement or in corner point grids. In this case there is a common contact area, $A_c$, between the volumes 2 and 3.

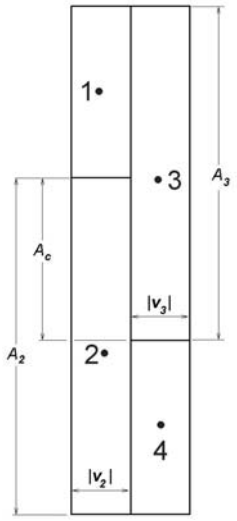


**Fig. 11 – Dimensions involved in transmissibility calculation between volumes 2 and 3**

According to equations (49) and (50), there are the resistances shown in Fig. 12 (*a*). It is interesting to note that the transmissibility calculation between the volumes 2 and 3 neglects the gray area of Fig. 12 *(b)*.

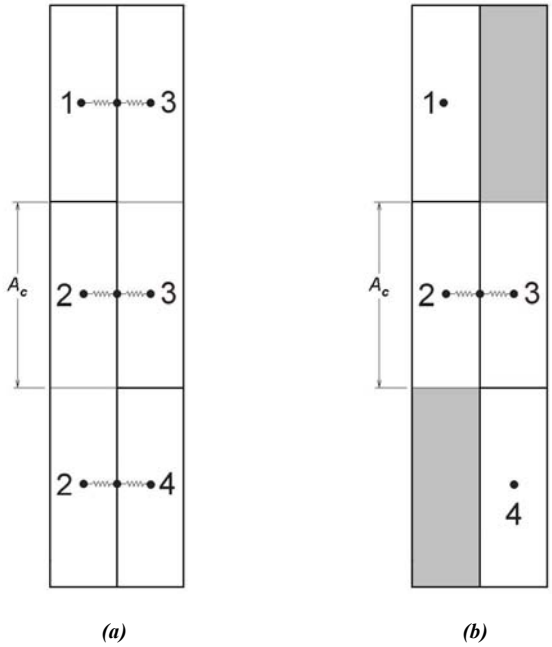


**Fig. 12 – *(a)* Resistance representative scheme used in simulators *(b)* gray areas that are neglected in the calculus of the transmissibility $T_{23}$**

Fig. 13 *(a)*, on the other hand, presents a grid where its volumes have partial contact with each other, i.e. the common contact area is not the total area of each volume. Actually, the grid that is being used, at least in terms of connectivity, is shown in Fig. 13 *(b)*, where it is shown three pairs of resistances involving three pairs of neighbor volumes. This is the geometrical situation interpreted by simulators, and it reproduces the analytical solution of a one dimensional problem.

In Appendix A, the numerical solution of a one dimensional heat transfer problem is presented. This problem has geometrical similarity with the porous media problem. It is demonstrated that the flux approximation by two-point scheme, as assumed in petroleum reservoir simulators, is the exact solution only for one-dimensional problems.

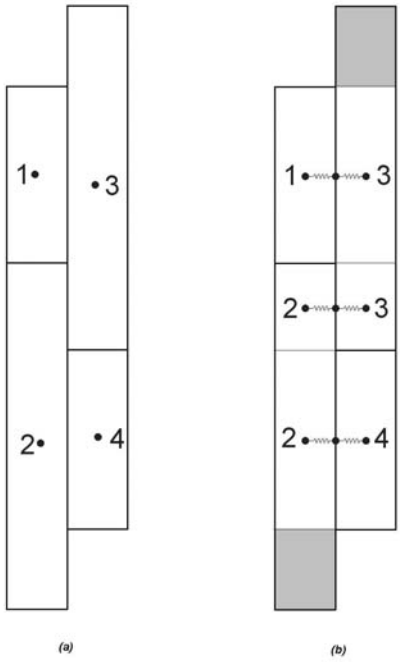


**Fig. 13 –** ***(a)*** **Corner point grid;** ***(b)*** **Resistance representative scheme used in simulators where the gray areas are not utilized in the calculus of transmissibilities**

### 3.2 – Considerations about transmissibility calculation in some of the most used grid types

In this section we consider the different schemes used to build the grids in most commercial simulators and how they affect the transmissibility determination. Theses schemes are related to the way the grid is built and is inputted to the software. Three different grid types will be considered: Cartesian, modified Cartesian and corner point. By modified Cartesian we understand the grid where the volumes are defined by the $z$ coordinate of the top surface. They are Cartesian volumes whose lateral surfaces may not match.

#### 3.2.1- Cartesian grids

In Cartesian grids, the area in transmissibility expression is the transversal flux area, i.e. for direction $x$, for example, the area is $\Delta y \Delta z$, while the length between centre-to-centre grid-point is $\Delta x$. Transmissibility calculation done in this way is exact, as already seen in this work and in Maliska *et al.* (2002*b*). Fig. 14 presents a Cartesian grid with non-uniform spacing between the cells.

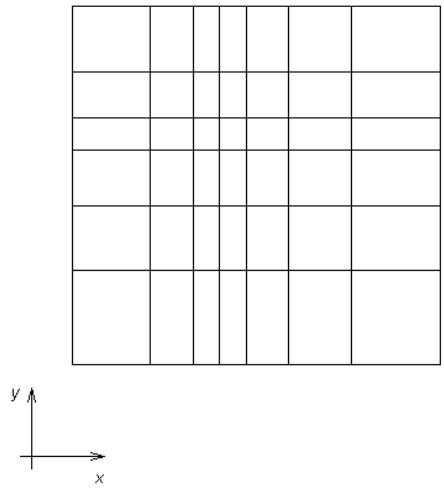


**Fig. 14 - Cartesian grid with non-uniform spacing**

#### 3.2.2 – Modified Cartesian grids

This grid is used in cases where we need a grid that presents layers of uniform thickness but with different depths. In this type of grid each column is shifted vertically. The area and the length used in the transmissibility expression, however, are the same used in Cartesian grids. Then, for the direction $x$, for example, the transmissibility is given by

$$T = \frac{\Delta Y \Delta Z}{\Delta X} k \tag{51}$$

Thus, we can have simulations which are at least "strange" as shown in Fig. 15. In this figure the reservoir with a constant inclination, Fig. 15*a*, was discretized by the blocks shown in Fig. 15*b*. Although the surfaces of the neighbor volumes are not in contact, in this model there is a mass flux between these surfaces, since the way transmissibility is defined permits it. The apparent no connection between the volumes can appear due to the use of a small quantity of volumes in the discretization and the reservoir dip. Actually, the simulator deals with the grid depicted in Fig. 15*b,* and with any grid built in this way, if it were as shown in Fig. 15*c*. In this approach, the fluid "disappears" in a point and "appears" in another point. The contacts, therefore, exist and the depth differences between the volumes are considered in the equations for the potential Φ. In other words, the grid is interpreted as the Cartesian of Fig. 15*c,* what demands a correction in the transmissibility values.

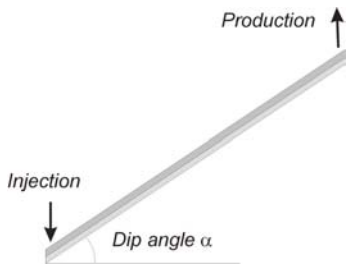


**Fig. 15** ***(a)***

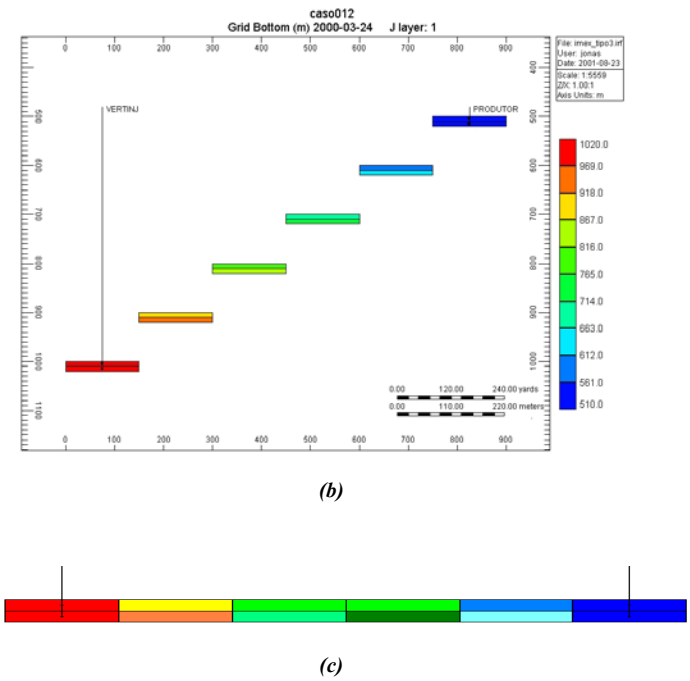


**Fig. 15 – Modified Cartesian grids used in simulations: *(a)* reservoir description; *(b)* grid utilized in the discretization, and *(c)* effective grid where the transmissibilities by simulators are calculated (from IMEX)**

Often commercial simulators permit to correct the transmissibility values already calculated by using transmissibility multipliers called *TRANSI*, *TRANSJ*, and so on, depending on the kind of simulator. For IMEX, Version 2002 User´s Guide, the default value is 1.

In these grids, when a simulator does not correct automatically the transmissibility value, it is recommend to multiply it by factor $\cos^2\alpha$. The reason is that the contacting cells centre-to-centre distance, as shown in Fig. 16, is $\Delta x/\cos\alpha$, and the transversal area to flux is now $\Delta y \Delta z \cos\alpha$. Thus, for this type of grids, with a constant dip, the transmissibility multiplier should be used, assuming the value $\cos^2\alpha$.

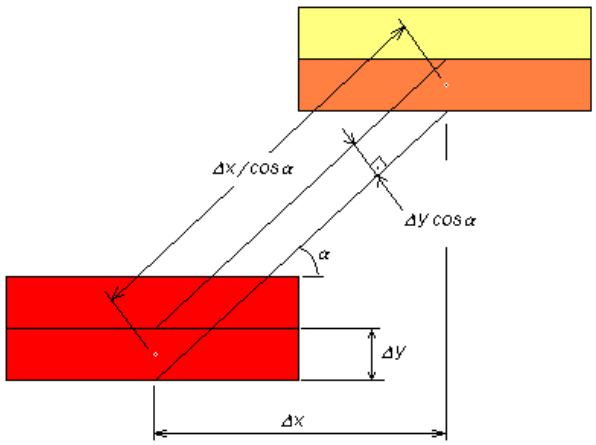


**Fig. 16 – Important geometrical parameters for the transmissibility calculation**

### 3.2.3 – Corner points grids

Another scheme that has been used in simulators for calculating transmissibilities is applied when corner point grids are employed. In this case, each grid-point should be given as input. The grid shown in Fig. 17 was built this way.

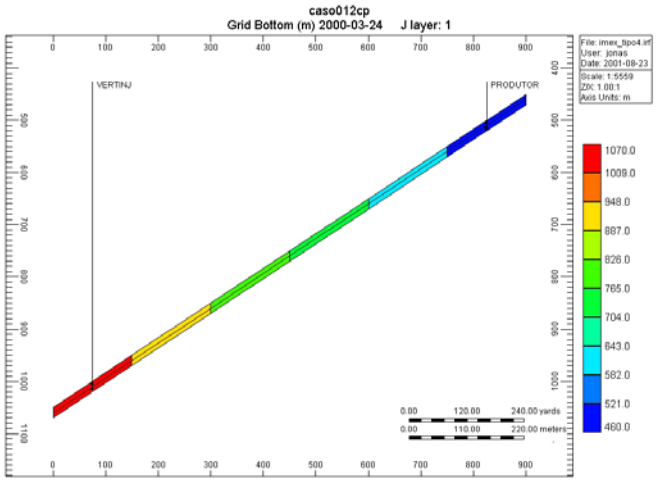


**Fig. 17 – Example of a corner point grid (from IMEX)**

The approach utilized for this type of grid is the same presented earlier in the section that discusses 3D grids. Hence, the simulators determine for each volume the distance between the two opposite face barycentres, the transversal area in the flux direction, and then the transmissibilities. As already mentioned, this is a good procedure (at least it is exact in a 1D problem). Therefore, the transmissibility multiplier should be the default value, which is 1.

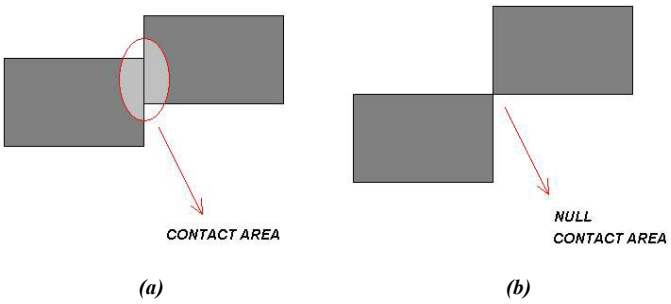


**Fig. 18 – Possible cases that can happen in corner points grids: (a) small contact area, and (b) null contact area**

The transversal area in the flux direction, which is utilized in the corner point grids transmissibility determination, is calculated by contact area of adjacent volumes. In Fig. 17, for example, the whole western surface of a volume is in contact with the whole eastern surface of another one. However, we can have situations like the one presented in Fig. 18*a*, where one observes that the contact area is smaller than the whole neighbor volumes surfaces. At the furthest extreme there is a case where the flux is zero since the neighbor volumes are not in physical contact (Fig. 18*b*).

A modified Cartesian grid can be built also by corner point grids if one uses the command *special connections*, likely found in most simulators. This command connects any two volumes, i.e. informs a value of transmissibility that will be used by the simulator between these volumes, even if they are not neighbors.

If in Fig. 19 the grid was built by corner points, the transmissibility in the *I* direction (the horizontal one) will be zero, and the flux will be zero. In order to use this grid, we need to calculate the transmissibility externally to the simulator, and input it into the simulator using the special connections command. We also should remember to correct this value by $\cos^2\alpha$.

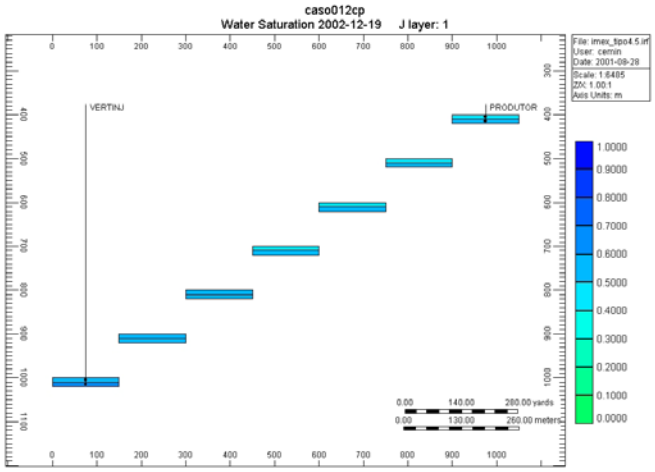


**Fig. 19 - Grid possible to be built by corner point definition. In this case one should use the special connections command.**

### 3.3 – Differences found in IMEX Transmissibility Calculation

This work presents several examples of transmissibility calculation using the commercial software IMEX (CMG) and the Sammon (2000) equations (described in section 3.1). The motivation for performing this comparison is that the results obtained using IMEX do not compare, in several cases, with the ones calculated using the Sammon's equation. These comparisons are embodied in a technical note to CMG by Maliska *et al.* (*2002a*).

To begin the presentation of the results, it is shown several cases where the transmissibilities calculated by IMEX plotted in the output file are coincident with those obtained by Sammon's equation. Figures. 20*a*, 20*b* and 20*c* present three of those cases. Fig. 20*d,* on the other hand, is a case where the transmissibility calculated by IMEX differs in 7.5% from the results obtained by the Sammon's equation.

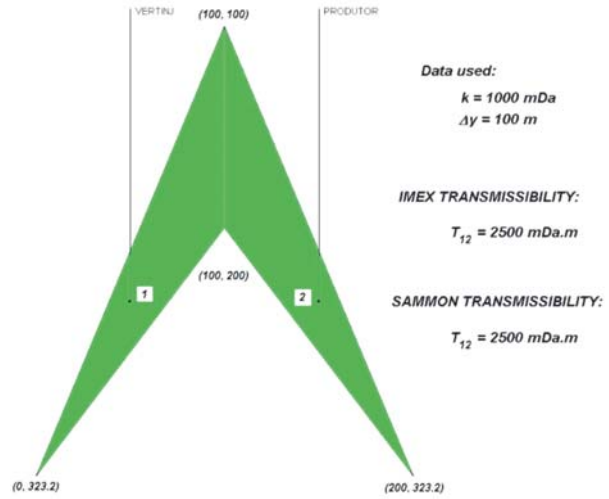


**Fig. 20** ***(a)***

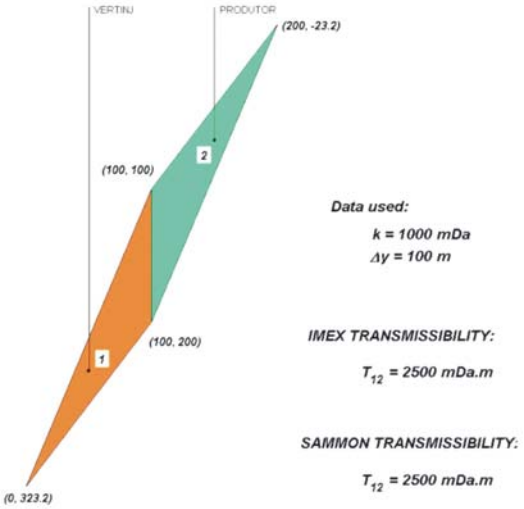


**Fig. 20** ***(b)***

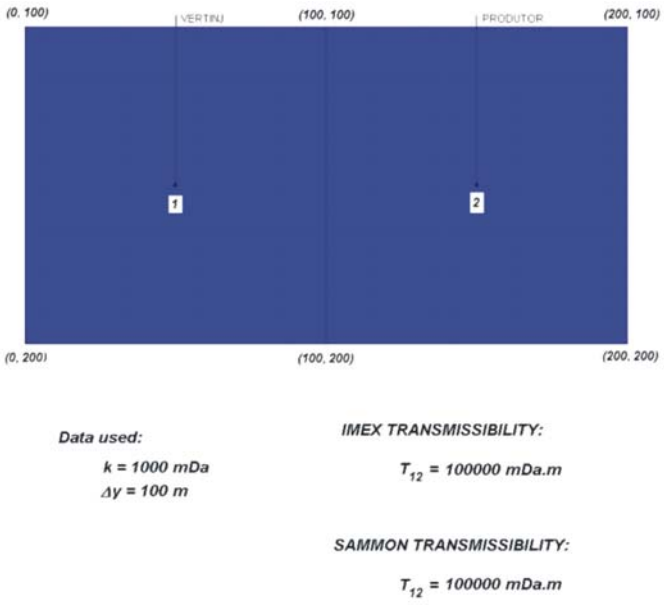


**Fig. 20** ***(c)***

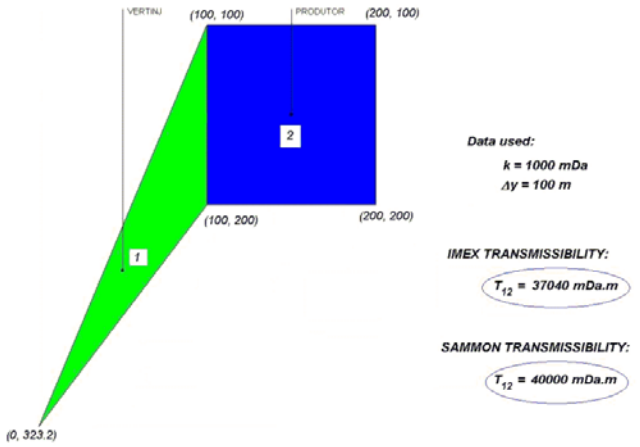


*(d)*

**Fig. 20 – Different grids with two blocks in contact: *(a)*, *(b)* and *(c)* the results of transmissibilities are coincident; (*d)* the result of IMEX transmissibility disagrees with that of Sammon**

In this section is done a qualitative study about these differences in cases commonly found in simulations. The percentage difference in transmissibility calculation is defined by

$$Difference\% = \left( \frac{T_{Sammon} - T_{Imex}}{T_{Sammon}} \right) 100 \qquad (52)$$

### 3.3.1 – Difference in transmissibilities values in function of lengths $d_1$, $d_2$ and angle $\alpha$

For the general case shown in Fig. 21 the relevant dimensions are the lengths $d_1$ and $d_2$, and the angle α.

From the results obtained, it is conclude that the differences are independent of both permeability and contact surface of volumes.

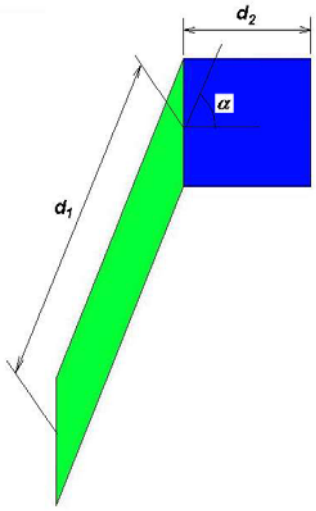


**Fig. 21 – Neighbor volumes with lengths $d_1$ and $d_2$**

Fig. 22 presents the percentage difference curves as a function of the relation $d_1/d_2$ and angle α. Note that the difference increases as angle α increases. For α = 80º and $d_1/d_2$ = 0.5, for example, the difference is, approximately, 45 %. With α = 60º and the same length relation, the difference decreases to, approximately, 10 %. The error is negligible for angles $\alpha$ less than 35º.

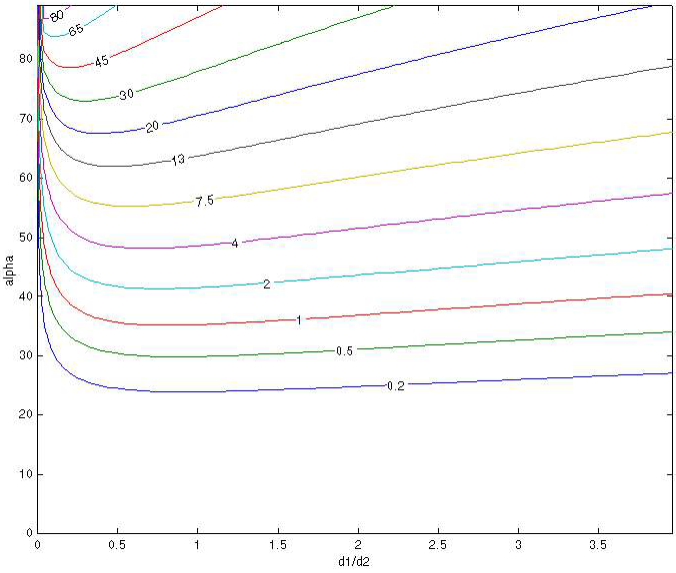


**Fig. 22 – Isolines of percentage differences as a function of angle $\alpha$ and the relation $d_1/d_2$**

### 3.3.2 - Differences in transmissibility as function of the angles $\alpha_1$, $\alpha_2$ and length $d$

For the general case shown in Fig. 23 the relevant dimensions are the angles $\alpha_1$ and $\alpha_2$, and the length $d$.

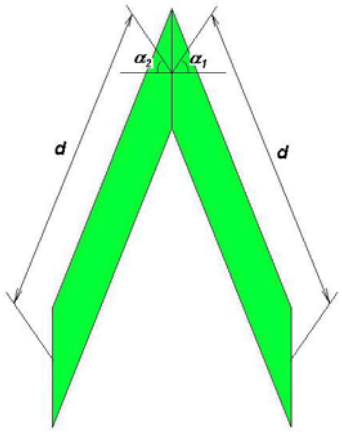


**Fig. 23 – Neighbor volumes with angles $\alpha_1$ and $\alpha_2$**

The results demonstrated that the differences are independent of permeability, and contact surface of volumes, and length $d$.

Fig. 24 presents the percentage differences curves as a function of angles $\alpha_1$ and $\alpha_2$ defined in Fig. 23. Note that the isolines are symmetric, i.e. the difference verified with $\alpha_1$ = 60º and $\alpha_2$ = 60º, for example, is identical to the configurations that follows

$\alpha_1$ = 60º and $\alpha_2$ = -60º
$\alpha_1$ = -60º and $\alpha_2$ = 60º
$\alpha_1$ = -60º and $\alpha_2$ = -60º

In any situation where $|\alpha_1| = |\alpha_2|$, the difference is zero.

Note that the differences are less than 1% and can be negligible in the region between the angles -30º and 30º (the central region of Fig. 24).

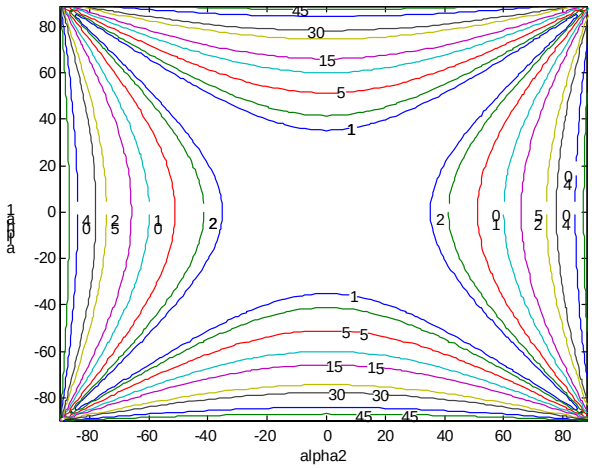


**Fig. 24 – Isolines of percentage differences as a function of angles $\alpha_1$ and $\alpha_2$**

### 3.3.3 - Differences in transmissibility as a function of $\alpha_1$, $\alpha_2$, $d_1$ and $d_2$

Finally, the analysis that follows is a general case and the relevant parameters, the lengths $d_1$ and $d_2$, and the angles $\alpha_1$ *and* $\alpha_2$ are shown in Fig. 25.

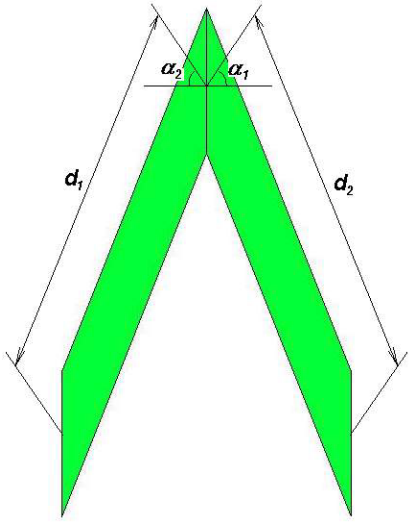


**Fig. 25 – Neighbor volumes with angles $\alpha_1$ and $\alpha_2$, and lengths $d_1$ and $d_2$, respectively**

Again, the differences in transmissibility are independent of permeabilities and contact area.

Fig. 26 shows the plot of percentage difference for the situation described in Fig. 25. The only care in using this figure to find out the error is to assign the subscript 1 to the volume that has the largest angle in relation to the horizontal plane, that is, $\alpha_1 \geq \alpha_2$

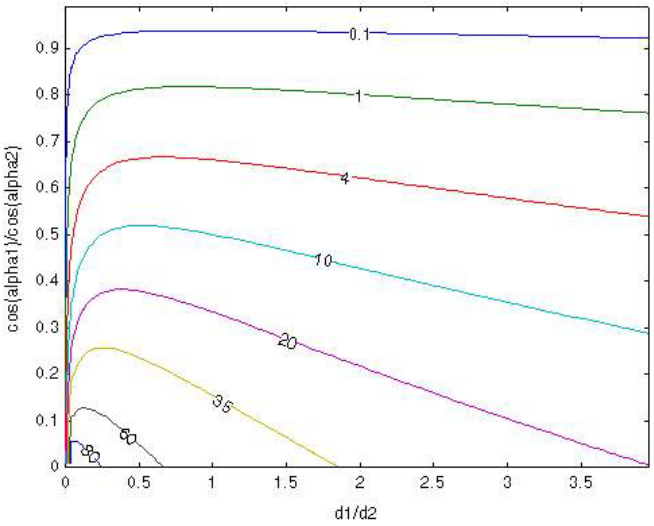


**Fig. 26 – Isolines of percentage differences for the situation described in Fig. 25. Using this figure the subscript 1 must be assigned to the volume that has the largest angle related to the horizontal plane, that is, ($\alpha_1 \geq \alpha_2$)**

## 4. Presentation of a EbFVM Method for reservoir simulation

As reported by Tamin *et al.,* 1999, a great amount of research was dedicated in the last decade in evaluating the available tools for numerical reservoir simulation. In contrast there was little efforts in developing new technologies and new approaches using conservative numerical schemes. Following, it is presented the ideas of a numerical reservoir simulator under development. It employs the ideas of Raw (1985) when developing the FIELD method for solution of the Navier-Stokes equations. It belongs to the class of the Element-based Finite Volume Methods (EbFVM) with new features for mobilities evaluation, relative and absolute permeabilities and local refinement near wells and/or faults. EbFVM is a better denomination for the method (Maliska 2003), also known as Control Volume Finite Element Method (CVFEM) since it is a finite volume methodology which borrows from the finite element technique the concept of elements. CVFEM would suggest a finite element formulations that obey the conservation principles at discrete level. However, these are called mixed finite element methods.

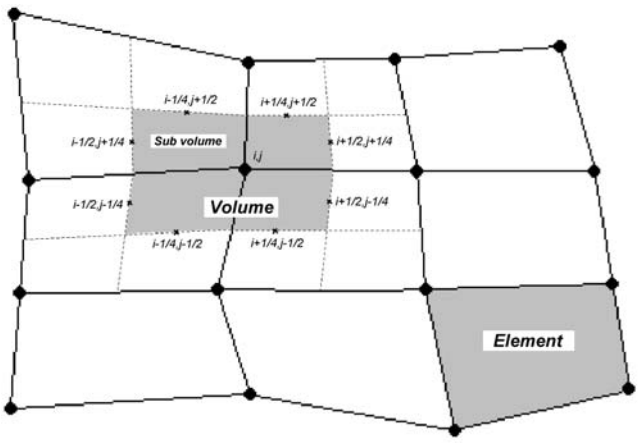


**Fig. 27 – Element, volume and sub-volume with integration points in a corner point grid**

The motivation for using this methodology is its flexibility, generality and clean computational implementation.

In a finite volume methodology the domain is covered by non-overlapping control volumes where the balances are done, as shown in Fig. 27. where an element is also defined. In the cell vertex construction, the control volumes are created joining the center of the elements to its medians. The resulting control volume is formed by portions (sub-control volumes) of neighboring elements. In this case, all fluxes at one specified integration point can be calculated using data from the element where the integration point lies. This allows the creation of the approximate equation for the unknown variable located at the center of the control volume which is formed by sub control volumes of the neighboring elements. Although this methodology can be generalized, to deal with triangular and quadrilateral elements, in this paper the equations will be presented only for quadrilateral elements.

The integration of the transient term of Eq. (1), for example, results in

$$\int_{svc} \frac{\partial(\phi S/B)}{\partial t} dV = V_{i,j} \frac{(\phi S/B)_{i,j}^{n+1} - (\phi S/B)_{i,j}^{n}}{\Delta t} \tag{53}$$

where $V_{i,j}$ is the total volume of control volume *i,j*, which is formed through the assembling of the sub-control volumes located near the node *i,j*.

The source term in Eq. (1), for example, in the sub-control volume of Fig. 27, located between points (*i,j*) and (*i+1/2,j+1/2*), yields

$$\int_{svc} q dV = q_{i+1/4,j+1/4} V_j \tag{54}$$

where $V_j$ is the volume of the sub-control volume where the integration is performed.

The integration of divergent term in Eq. (1) yields

$$\int_V \nabla.(\lambda_m k \nabla p) dV = \sum_{k=1}^{8} \int_{\Gamma_i} \lambda_i k \frac{\partial p}{\partial \mathbf{n}} d\sigma \tag{55}$$

that corresponds to the evaluation at the integration points in Fig. 27, located in the center of the sub-control volumes surfaces. For the integration point (*i+1/2, j-1/4*), for example, this term is written as

$$\int_{p(i+1/2,j-1/4)} (\lambda_m k \nabla p) d\mathbf{s} = \int_{p(i+1/2,j-1/4)} (\lambda_m k \nabla p).(dy\mathbf{i} - dx\mathbf{j}) \tag{56}$$

or

$$= \int_{p(i+1/2,j-1/4)} \left(\lambda_m k \frac{\partial p}{\partial x}\right) dy - \int_{p(i+1/2,j-1/4)} \left(\lambda_m k \frac{\partial p}{\partial y}\right) dx \tag{57}$$

and, integrating this expression one gets

$$= \left(\lambda_m k \frac{\partial p}{\partial x}\right)_{i+1/2,j-1/4} \Delta y - \left(\lambda_m k \frac{\partial p}{\partial y}\right)_{i+1/2,j-1/4} \Delta x \tag{58}$$

where the last term disappears in Cartesian grids. Even in such particular case, this method results in a nine-point scheme for the pressure. The use of nine-point scheme has been considered a desirable feature in numerical methods in order to reduce grid orientation effect (Yanopsik and McCracken, 1979) (Ko and Au, 1979) (Shiralkar and Stephenson, 1987).

We propose a bi-linear variation for pressure, for quadrilateral elements in the form

$$P = N_1 P_{i,j} + N_2 P_{i,j+1} + N_3 P_{i+1,j+1} + N_4 P_{i+1,j} \tag{59}$$

where the operators $N_i$ are the shape functions defined by

$$\begin{aligned} N_1(s,t) &= \frac{1}{4}(1+s)(1+t) \\ N_2(s,t) &= \frac{1}{4}(1-s)(1+t) \\ N_3(s,t) &= \frac{1}{4}(1-s)(1-t) \\ N_4(s,t) &= \frac{1}{4}(1+s)(1-t) \end{aligned} \tag{60}$$

Using a local coordinate for each element, allows each element and volume to become independent of other elements and volumes. The domain of this local coordinate system (*s,t*) should vary from -1 to +1, and the nodes should be ordered from 1 to 4 (in a anticlockwise direction), as shown in Fig. 28

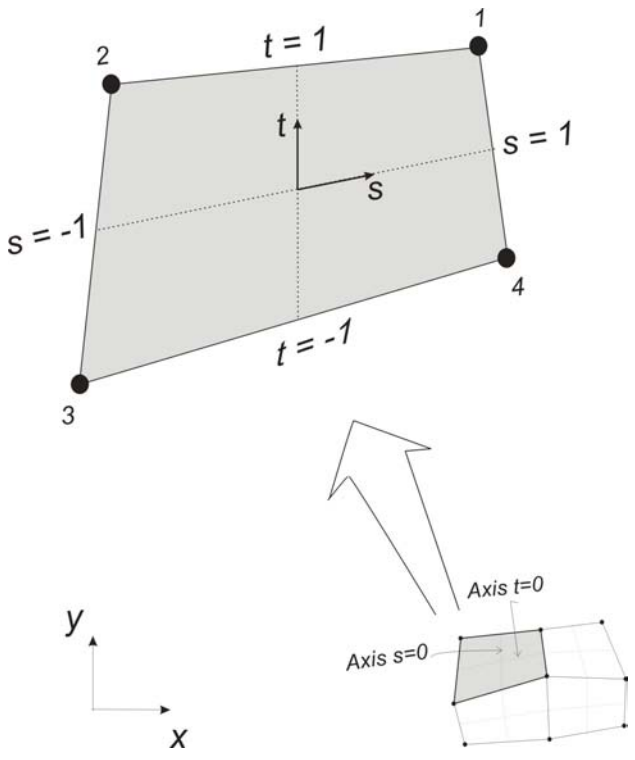


**Fig. 28 – Local coordinate system**

If $x_i$ and $y_i$ are the global coordinates of node $i$, any coordinates $x$ and $y$ of any element internal point can be determined by

$$x(s,t)=\sum_{i=1}^{4} N_i(s,t)x_i \tag{61}$$

and

$$y(s,t)=\sum_{i=1}^{4} N_i(s,t)y_i \tag{62}$$

Due to the continuity of the shape functions in the element, its derivative can be performed as

$$\left.\frac{\partial P}{\partial x}\right|_{s,t}=\sum_{i=1}^{4}\left.\frac{\partial N_i}{\partial x}\right|_{s,t} P_i \tag{63}$$

and

$$\left.\frac{\partial P}{\partial y}\right|_{s,t}=\sum_{i=1}^{4}\left.\frac{\partial N_i}{\partial y}\right|_{s,t} P_i \tag{64}$$

In order to obtain the shape functions derivatives $\partial N_i/\partial x$ and $\partial N_i/\partial y$, one uses the chain rule

$$\frac{\partial N_i}{\partial s}=\frac{\partial N_i}{\partial x}\frac{\partial x}{\partial s}+\frac{\partial N_i}{\partial y}\frac{\partial y}{\partial s} \tag{65}$$

and

$$\frac{\partial N_i}{\partial t}=\frac{\partial N_i}{\partial x}\frac{\partial x}{\partial t}+\frac{\partial N_i}{\partial y}\frac{\partial y}{\partial t} \tag{66}$$

tSolving this system one gets

$$\frac{\partial N_i}{\partial x}=\frac{1}{J}\left(\frac{\partial N_i}{\partial s}\frac{\partial y}{\partial t}-\frac{\partial N_i}{\partial t}\frac{\partial y}{\partial s}\right) \tag{67}$$

and

$$\frac{\partial N_i}{\partial y}=\frac{1}{J}\left(\frac{\partial N_i}{\partial t}\frac{\partial s}{\partial s}-\frac{\partial N_i}{\partial s}\frac{\partial x}{\partial t}\right) \tag{68}$$

where $J$ is the Jacobian given by

$$J=\frac{\partial x}{\partial s}\frac{\partial y}{\partial t}-\frac{\partial x}{\partial t}\frac{\partial y}{\partial s} \tag{69}$$

The derivatives of $Ni$, $x$ and $y$ in relation to $s$ and $t$ can be obtained in Cordazzo (2002).

Therefore the fluxes balance in the volume $i,j$ given in Fig. 27 is given by

$$\int_V \nabla.(\lambda_m k\nabla p)dV=\sum_{k=1}^{8}\int_{\Gamma_i}\lambda_i k\frac{\partial p}{\partial \mathbf{n}}d\sigma=$$

$$=\lambda_{i+1/2,j-1/4}(a_1p_{i+1,j}+a_2p_{i+1,j-1}-a_3p_{i,j}-a_4p_{i,j-1})+$$

$$+\lambda_{i+1/4,j-1/2}(b_1p_{i+1,j}+b_2p_{i+1,j-1}-b_3p_{i,j}-b_3p_{i,j-1})+$$

$$+\lambda_{i+1/2,j+1/4}(c_1p_{i+1,j+1}+c_2p_{i+1,j}-c_3p_{i,j}-c_4p_{i,j+1})+$$

$$+\lambda_{i+1/4,j+1/2}(d_1p_{i+1,j+1}+d_2p_{i+1,j}-d_3p_{i,j}-d_4p_{i,j+1})+$$

$$+\lambda_{i-1/4,j+1/2}(e_1p_{i,j+1}+e_2p_{i,j}-e_3p_{i+1,j-1}-e_4p_{i-1,j})+$$

$$+\lambda_{i-1/2,j+1/4}(f_1p_{i,j+1}+f_2p_{i,j}-f_3p_{i-1,j+1}-f_4p_{i-1,j})+$$

$$+\lambda_{i-1/2,j-1/4}(g_1p_{i,j-1}+g_2p_{i,j}-g_3p_{i-1,j-1}-g_4p_{i-1,j})+$$

$$+\lambda_{i-1/4,j-1/2}(h_1p_{i,j-1}+h_2p_{i,j}-h_3p_{i-1,j-1}-h_4p_{i-1,j}) \tag{70}$$

where $a_i$, $b_i$, $c_i$, $d_i$, $e_i$, $f_i$, $g_i$ and $h_i$ are constants depending only on the grid and permeability.

The mobility evaluation is another important point to be dealt with besides the correct flux calculation offered by the method. Grid orientation effect reduction is sometimes associated with schemes of mobility evaluation (Todd *et al*., 1972) (Vinsome and Au, 1979) (Frauenthal and Towler, 1985). In the following section, the procedure adopted in the proposed method to estimate the mobility $\lambda$ in the integration points is discussed.

### 4.1 – Mobility determination at the integration points

If the mobilities $\lambda$ are evaluated as a function of the four node properties in quadrilateral elements (or three in triangular elements), the resulting scheme will be of nine-point also for mobility. Most of the works in the literature use upstream scheme in order to evaluate the mobilities. Even in those using non-structured grids, the procedure is similar and can be summarized in the form

$$\lambda_{12}=\lambda_1 \qquad \text{if } \lambda_1>\lambda_2$$

$$\lambda_{12}=\lambda_2 \qquad \text{if } \lambda_2>\lambda_1$$

where $\lambda_{12}$ is the mobility evaluated in the integration point located between points 1 and 2. Due to the alignment of mobility with the gridlines instead of flux direction, this procedure can generate excessive numerical diffusion. Several results in the literature demonstrate the need of treating more accurately the mobility terms. (Yoshiaki, 1982)(Wolcott *et al.,* 1996).

In this paper, it is proposed to use the skew method already used by Souza (2000) for evaluating the convective terms of the Navier-Stokes equations. The method, called suds-no (*skew upstream difference scheme-node*), is a simplification of the suds (*skew upstream difference scheme*)

proposed originally by Raw (1985). These schemes identify the flux direction and apply the interpolation function in alignment with the stream lines. In Fig. 29, the stream line *s* depicts the preferential flux direction. The interpolation function applied in this direction warranties that even in flows with vortices, the variable is always evaluated in the correct position. This is an important feature since we have found some works confirming that the grid orientation effect is a result of a convective phenomenon (Sonier and Eymard, 1993).

For the integration point $pi_1$ in Fig. 29, for example, the mobility utilized is that evaluated in point $p_1$, located between the nodes 2 and 3.

In this way, the mobility in integration point $pi_1$ is given by

$$\lambda_{pi_1} = \lambda_{p_1} \tag{71}$$

where $\lambda_{p_1}$ is the mobility in point $p_1$, which is determined by the mobilities calculated with nodes 2 and 3:

$$\lambda_{p_1} = \frac{a}{b}\lambda_2 + \left(1 - \frac{a}{b}\right)\lambda_3 \tag{72}$$

where *a* and *b* are the lengths defined in Fig. 29. When the mass flux goes into the sub-control volume, the mobility in the integration point $pi_1$ will be estimated by the values at 1 and 2 nodes when the stream line *s* intercepts the top surface. When the stream line intercepts the bottom surface, the values used will be of nodes 3 and 4. Identical formulations should be created for the cases where the mass goes out of the sub-control volume.

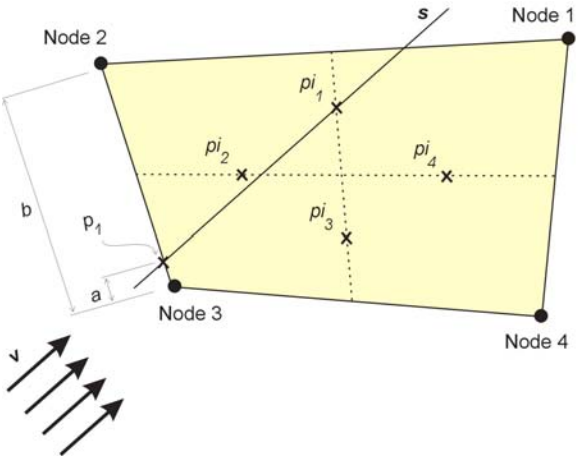


**Fig. 29 – Mobility evaluation scheme**

The procedure applied to other integration points and to triangular elements is similar. In a three dimensional case, on the other hand, the mobility value in the integration point involves the four nodes belonging to the surface intercepted by the stream line. Fig. 30*(a)* and *(b)* depict the procedure applied to three dimensional problems, showing a corner sub-control volume and an internal volume, respectively. In both figures, for the sake of exemplification, the mobility is evaluated as function of nodes 1, 2, 3 and 4.

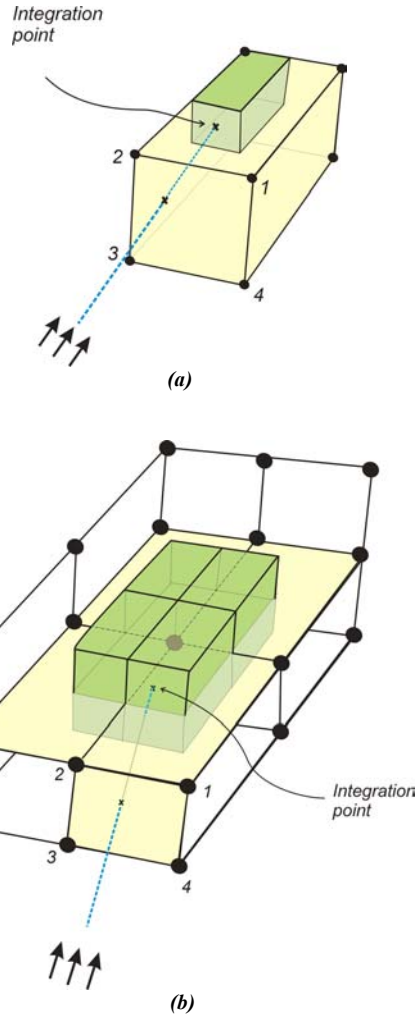


**Fig. 30 – Mobilities evaluation scheme, for *(a)* the corner sub control volume, and *(b)* the internal sub control volumes, in the three-dimensional case**

The shape function $N_i$ for 3D (hexahedra) can be found in Chung (1981).

For the vertical direction, however, the same flux approximation scheme commonly utilized in most reservoir simulators (by two points), will be used here. This scheme was already used by Kuwauchi *et al*. (1996), for example, in the simulator VERDI3D, where the equation was integrated in the horizontal (areal) plane using Voronoi's grids. This scheme was called *pseudo-three-dimensional* or *2.5 three-dimensional.* The justification for using this approach is the reservoir geometry.

## 5. Conclusions

In this paper it was discussed important aspects related to the type of grids used in petroleum reservoir simulation. The transmissibility definition and its proper calculation were analyzed in the framework of boundary-fitted method. The use of the two-point approximation approach, largely used in commercial simulators was also discussed. It clear that only

when locally orthogonal grids and in 1D situations the two-point approach yields exact results.

Comparisons using a commercial simulator and the equation of Sammon were presented, showing that in some cases the errors can be significant. The error was plotted against geometrical parameters.

Finally, a new numerical scheme to simulate petroleum reservoir was presented. It is based in the EbFVM (Element based Finite Volume Method), and it can use mixed triangular and quadrilateral elements. The proposed method retains the geometric flexibility of the finite-element procedure and derives the governing discrete algebraic equations by using a conservation balance applied to discrete control volumes laid-out throughout the domain. In this method the transmissibility terms are embodied in the coefficients and are not individually identified. It results in a nine-point scheme for both the pressure and the mobility, and this is a desired characteristic because they reduce the grid orientation effect.

## 6. References


CHUNG, T. J., 1981. *Introduction to Finite Element Analysis in Fluids and Heat Transfer*, in Finite Element Methods in Continuum Mechanics, Volume 1, The University of Alabama, Huntsville, Alabama.

CORDAZZO, J., 2002. *PhD Qualifying,* in Portuguese, Department of Mechanical Engineering, Federal University of Santa Catarina, Florianopolis, SC, Brazil.

FRAUENTHAL, J. C., di Franco, R. B., and TOWLER, B. F. T., 1985. *Reduction of Grid-Orientation Effects in Reservoir Simulator with Generalized Upstream Weighting*. SPE paper 11593, Society of Petroleum Engineers Journal.

HEGRE, T. M., DALEN, V. & HENRIQUEZ, A., 1986. *Generalizes Transmissibilities for Distorted Grids in Reservoir Simulation.* Paper SPE 15622 presented at the 61st Annual Tech. Conf. Exh. of SPE (New Orleans, Oct. 5-8).

HEINEMANN, Z. E. & BRAND, C. W., 1989. *Gridding Techniques in Reservoir Simulation.* 1st/2nd Stanford Univ. & Leoben Mining Univ. Reservoir Simulation Inf. Forum (Alpbach, Austria, Sept/1998-Sept/1989).

IMEX, *Version 2002 User's Guide*. Computer Modelling Group Ltd, Calgary, Alberta, Canada.

KO, S. C. M. and AU, A. D. K. 1979. *A Weighted Nine-Point Finite-Difference Scheme for Eliminating the Grid Orientation Effect in Numerical Reservoir Simulation.* SPE paper 8248 presented at the 54th Annual Fall Technical Conference and Exhibition, Las Vegas, Nevada, September 23-26.

KUWAUCHI, Y, ABBASZADEH, M., SHIRAKAWA, S., and YAMAZAKI, N., 1996. *Development and Applications of a Three Dimensional Voronoi-Based Flexible Grid Black Oil Reservoir Simulator,* SPE paper 37028 presented at the SPE Asia Pacific Oil & Gas Conference, Adelaide, Australia, 28-31 October.

MALISKA, C. R., 2001. *Volumetric Grids for Petroleum Reservoir Simulation*, 1st report, in Portuguese, Project 6502077013, Laboratory of Numerical Simulation, UFSC, Florianopolis, SC, Brazil.

MALISKA, C. R., da SILVA., A. F. C., CORDAZZO, J. and CEMIN, A., 2002*a*. *Comparison of the Transmissibility Calculated by IMEX and Those obtained using Sammon's Equations*, Technical Note to CMG. Laboratory of Numerical Simulation, UFSC, Florianopolis, SC, Brazil.

MALISKA, C. R., da SILVA., A. F. C., CORDAZZO, J. and CEMIN, A., 2002*b*. *Volumetric Grids for Petroleum Reservoir Simulation*, 4st report, in Portuguese, Project 6502077013, Laboratory of Numerical Simulation, UFSC, Florianopolis, SC, Brazil.

MALISKA, C.R., 1995. *Heat Transfer and Computational Fluid Dynamics – Fundamentals and Boundary Fitted*, 424p, 1st edition, in Portuguese, Livros Técnicos e Científicos Editora, Rio de Janeiro, Brazil.

MALISKA, C.R., 2003. *Numerical Heat Transfer and Fluid Flow*, 2nd edition, in Portuguese, in press, Livros Técnicos e Científicos Editora, Rio de Janeiro, Brazil.

PONTING, D. K., 1989. *Corner Point Geometry in Reservoir Simulation*, Proc. 1st European Conference on the Mathematics of Oil Recovery, Cambridge, United Kingdom.

RAW, M., 1985. *A New Control Volume Based Finite Element Procedure for the Numerical Solution of the Fluid Flow and Scalar Transport Equations*, Ph.D. Thesis, University of Waterloo, Waterloo, Ontario, Canada.

SALAZAR, V., 2002. *Personal communication*. CMG South America, Las Mercedes, Caracas, Venezuela.

SAMMON, P. H., 2000. Calculation of Convective and Dispersive Flows for Complex Corner *Point Grids*. Paper SPE 62929, Computer Modelling Group, Ltd.

SHIRALKAR, G. S. and STEPHENSON, R. E., 1987. *A General Formulation for Simulating Physical Dispersion and a New Nine-Point Scheme*, SPE paper 16975 presented at the 62nd Annual Technical Conference and Exhibition of the Society of Petroleum Engineers, Dallas, TX, September 27-30.

SONIER, F. and EYMARD, R., 1993. *Mathematical and Numerical Properties of Control-Volume Finite Element Scheme for Reservoir Simulation,* SPE paper 25267 presented at 12th SPE Symposium on Reservoir Simulation, New Orleans, LA, U.S.A., February 28-March 3.

SOUZA, J. A., 2000. *Implementation of a Finite Volume with Local Coordinates for Method for the Coupled Solution of Navier-Stokes Equations*, Master Thesis in Portuguese, Department of Mechanical Engineering, Federal University of Santa Catarina, UFSC, Florianopolis, SC, Brazil.

TAMIN, M., ABOU-KASSEM, J. H. and FAROUQ ALI, S. M., 1999. *Recent Developments in Numerical Simulation Techniques of Thermal Recovery*, SPE paper 54096 presented at the SPE International Thermal Operations and Heavy Oil Symposium, Bakersfield, California, 17-19 March.

TODD, M. R., O´DELL, P. M., and HIRASAKI, G. J., 1972. *Methods for Increased Accuracy in Numerical Reservoir Simulators*. Soc. Pet. Eng. J., Dec., 515-530.

VINSOME, P. K. and AU, A. D. K., 1979. *One Approach to the Grid Orientation Problem in Reservoir Simulation.*

SPE paper 8247 presented at the 54th Annual Fall Technical Conference and Exhibition, Las Vegas, Nevada, September 23-26.

WOLCOTT, D. S., KAZEMI, H. and DEAN, R. H., 1996. *A Practical Method for Minimizing the Grid Orientation Effect in Reservoir Simulation*. SPE paper 36723 presented at the SPE Annual Technical Conference and Exhibition, Denver, Colorado, USA, 6-9 October.

YANOSIK, J. L. and McCRACKEN, T. A., 1979. *A Nine-Point Finite-Difference Reservoir Simulator for Realistic Prediction of Adverse Mobility Ratio Displacements*. SPEJ, Aug., 253-262; Trans., AIME, **267**.

YOSHIAKI, I., 1982. *Evaluation of Interblock Mobility Using a Modified Midpoint Weighting Scheme*, SPE paper 10498 presented at the 6th SPE Symposium on Reservoir Simulation, New Orleans, LA, January 31-February 3.

## 7. Acknowledgements

The authors are grateful to CENPES/Petrobras, Agência Nacional do Petróleo (ANP) and FINEP for the financial support of this work. The authors would like to thank also the graduation students Angelo Cemin, Rafael Mendes and Rodrigo Ferraz for their help in parts of this work.

## Appendix A – Study of the Transmissibilities by physical similarity with heat transfer problems

Transmissibility calculation in mass transfer problems depends on both physical properties in the control volume interfaces and geometrical factors. We can, therefore, establish an analogy between the conductance ($U$) of heat transfer problems and the transmissibility ($T$) of transport problems in porous media.

The conservation equation of energy, in a steady state, is given by

$$\nabla \cdot (k \cdot \nabla T) + S = 0 \qquad \text{(A1)}$$

where $k$ represents the conductivity and $S$ is the source term related to a possible energy generation. Integrating Eq. (A1) in control-volume, and after the application of divergence theorem, this equation yields

$$\sum_{i=interfaces} \left( k \frac{\partial T}{\partial \vec{n}} \right)_{Pi} \Delta S_{Pi} + S \cdot \Delta V = 0 \qquad \text{(A2)}$$

where the term into brackets represents the heat flux by unit of area between two adjacent control-volumes, and $\Delta S_{Pi}$ represents the interface area between these control-volumes.

The term

$$\left( k \frac{\partial T}{\partial \vec{n}} \right)_{Pi} \Delta S_{Pi}$$

represents the flux that goes through the interface. This term can be written as $U(T_P - T_i)$, where $U$ is the conductance or transmissibility between two adjacent blocks $P$ and $i$, and the difference between the temperatures $(T_P - T_i)$ has the analogy with the potential difference $(\phi_P - \phi_i)$ for mass transfer problems.

Therefore, Eq. (A2) can be rewritten as

$$\sum_{i=interfaces} U_{Pi}(T_P - T_i) + S \cdot \Delta V = 0 \qquad \text{(A3)}$$

The great difficult to solve the problems is the exact determination of the conductance $U_{Pi}$ between two blocks. As already stated, if $U$ is deduced directly from differential equation in a conservative form, there is not difficulties since the determination, in this way, is done directly from the approximate equation.

### A1 – Transmissiblity study by 1D problems

Fig. A1 shows a 1D heat transfer problem that will be solved analytically and numerically.

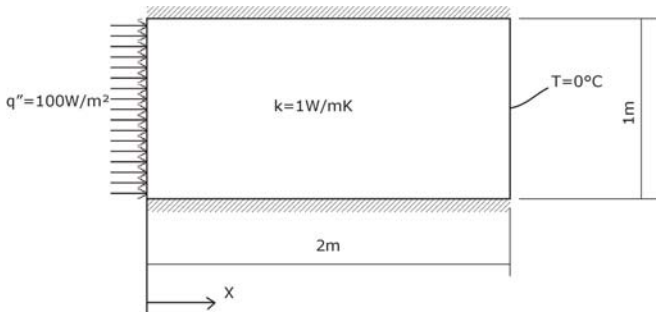


**Fig. A1– 1D heat transfer problem**

It is easy to show that the solution of the problem defined in Fig. A1 is given by

$$T(x) = -100x + 200 \qquad \text{(A4)}$$

In order to obtain the numerical solution, the problem was discretized using the grid presented in Fig. A2, where the dimensions $H$ and $L$ are, in this case, 1 m and 2 m, respectively.

Observe that the grid presents control-volumes in contact with more than one volume in the direction $x$. This arrangement permits applying several models of transmissibility calculation. (3.3)

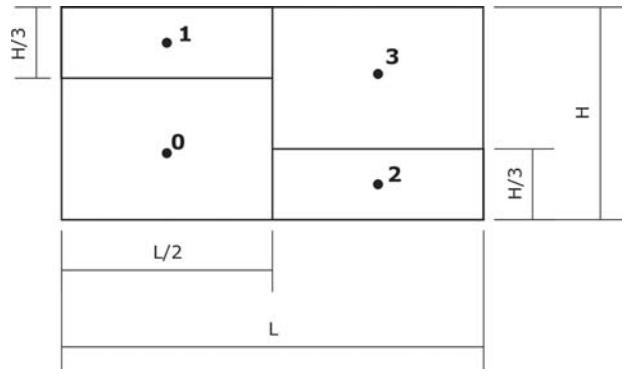


**Fig. A2 – Discretization of 1D Heat transfer given in Fig. A1**

Three models to calculate conductance will be presented. Model 1D-1 uses the concept of two resistances in series, where each one is calculated by the information of its own control-volume, as shown in Fig. A3. This model is called "electrical resistance model" and it will be used also in 2D problems. Model 1D-2, on the other hand, uses the tubular area, as shown in Fig. A4, and Model 1D-3 uses all the transversal area to flux, as depicted in Fig. A5. After the presentation of these models, it is done a comparison between the results and the analytical solution. The physical parameter ($k$) in the conductance is constant for all volumes.

***Model 1D-1: Electrical resistance model***

In this model the resistances are calculated for each volume and the total resistance is the sum of these resistances in series. The areas used are the same for two volumes, and the lengths are indicated in the bottom of the Fig. A3, which goes through the volume centre to the center of the contact surface.

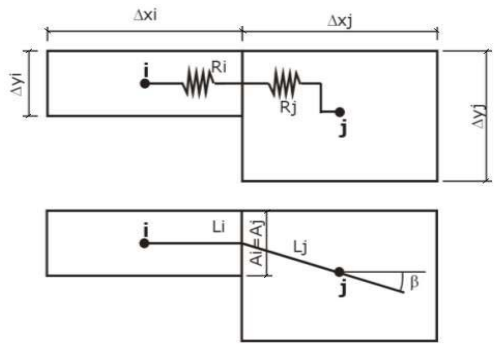


**Fig. A3 - Model 1D-1: based on electrical resistances**

Therefore, the equivalent resistance $R_e$ is given by

$$R_e = R_i + R_j = \frac{\Delta x_i}{2 \cdot k \cdot \Delta y_i} + \frac{\Delta x_j / \cos(\beta)}{2 \cdot k \cdot \Delta y_i} \qquad \text{(A5)}$$

and the conductance between the volumes $i$ and $j$, $U_{ij}$, yields

$$U_{ij} = \frac{1}{R_e} = \frac{2 \cdot k \cdot \Delta y_i}{\Delta x_i + \Delta x_j / \cos(\beta)} \qquad \text{(A6)}$$

***Model 1D-2: Using the "Tubular" area***

According to this model, the area to be used is the tubular area, $A_{ij}$, which is presented in Fig. A4.

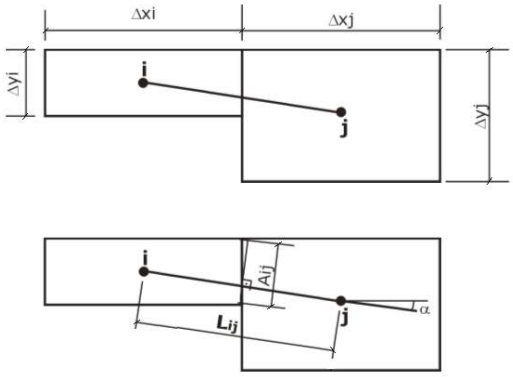


**Fig. A4 - Model 1D-2 for conductance calculation: tubular area**

In this model the conductance is given by

$$U_{ij} = \frac{k \cdot A_{ij}}{L_{ij}} \qquad \text{(A7)}$$

In a case where the grid is uniformly spaced ( $\Delta x_i = \Delta x_j$ ), and observing that

$$A_{ij} = \Delta y_i \cdot \cos(\alpha) \cdot 1 \qquad \text{and} \qquad L_{ij} = \Delta x_j / \cos(\alpha)$$

the equation (A7) results

$$U_{ij} = \frac{k \cdot \Delta y_i \cdot \cos(\alpha)}{\Delta x_j / \cos(\alpha)} = \frac{k \cdot \Delta y_i}{\Delta x_j} \cdot \cos^2(\alpha) \qquad \text{(A8)}$$

***Model 1D-3: Using all transversal area to flux***

In this case, the only difference from Model 1D-2 is the utilization of all transversal area to flux $A_{ij}$ (shown in Fig. A5) in the conductance expression.

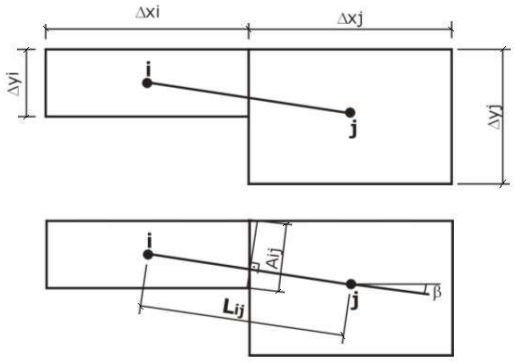


**Fig. A5 - Model 1D-3 for conductance calculation: using all transversal area**

Assuming also a uniformly spaced grid ( $\Delta x_i = \Delta x_j$ ),

$$A_{ij} = \left(\Delta y_i / \cos(\alpha)\right) \cdot 1 \qquad \text{and} \qquad L_{ij} = \Delta x_j / \cos(\alpha)$$

the equation (A7) results

$$U_{ij} = \frac{k \cdot \Delta y_i / \cos(\alpha)}{\Delta x_j / \cos(\alpha)} = \frac{k \cdot \Delta y_i}{\Delta x_j} \tag{A9}$$

***Comparison of results***

In Tab. A1 are compared the temperature values for the volumes 0, 1, 2 and 3 shown in Fig. A2, with the analytical solution.

**Tab. A1 – Temperature values obtained from several models**

| Solution | $T_0$ (°C) | $T_1$ (°C) | $T_2$ (°C) | $T_3$ (°C) |
|---|---|---|---|---|
| | | | | |
| Analytical | *150* | *150* | *50* | *50* |
| Model 1D-1 | *153.6552* | *153.5182* | *50.0809* | *49.9672* |
| Model 1D-2 | *155.5558* | *155.1527* | *50.2283* | *49.8889* |
| Model 1D-3 | *150* | *150* | *50* | *50* |

Note that the solution of the third model, i.e. which utilized all transversal area in the calculus, is the exact solution of this problem. The second model (tubular area), on the other hand, presented the worst errors.

Model 1D-3 is the model adopted for transmissibility calculation in most commercial simulators.

## A2 – Transmissibility study in 2D problems

In this section we investigate different models to calculate transmissibilities in 2D problems. A heat transfer problem that has analytical solution is used again. This problem is depicted in Fig. A6. In the direction *z* the plate thickness is 1.

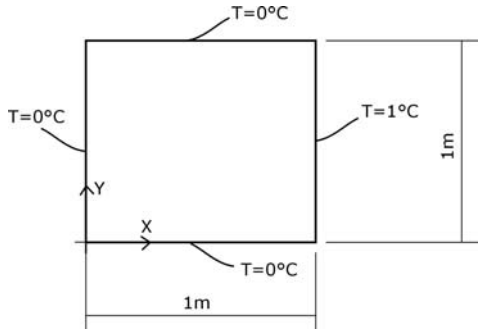


**Fig. A6 - 2D heat transfer problem**

This problem has an analytical solution which permits an accurate evaluation of different methods of transmissibility calculation. The analytical solution, obtained by the separation of variables method, is given by

$$T(x,y) = \frac{2}{\pi} \sum_{n=1}^{\infty} \frac{(-1)^{n+1} + 1}{n} sen(n\pi(1-y)) \frac{senh(n\pi x)}{senh(n\pi)} \tag{A10}$$

For the numerical study, the domain was discretized using Cartesian grids with local refinement, such as shown in Fig. A7. This type of local refinement originates the condition where a control volume's face has contact with other two volumes. So, there are different ways to calculate the transmissibility which will be investigated through the use of a coarse grid, Fig. A7*(a)*, that has 5x5 volumes and a fine grid, Fig. A7*(b)*, that has 21x21 volumes. The columns are locally refined with a multiplier factor 2.

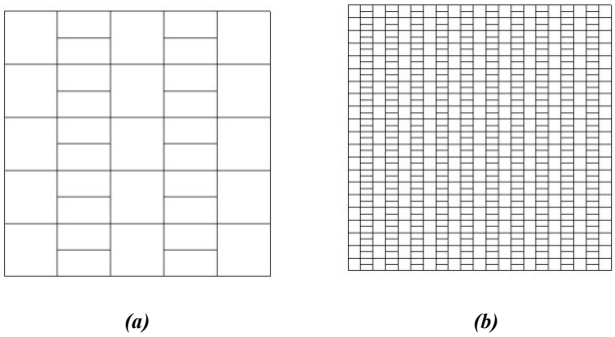


**Fig. A7 – Grids with local refinement utilized for resolution of 2D problem: *(a)* with 5x5 volumes and *(b)* with 21x21 volumes**

We will investigate four different models in order to determine the transmissibilities:

. Model 2D-1: uses Sammon's equation (2000)
. Model 2D-2: uses the correction factor $\cos^2 \beta$
. Model 2D-3: uses the Voronoi grid
. Model 2D-4: uses the Electrical resistance model

Here, again, all models can be interpreted as an electrical resistance model. However, we identify the fourth model as the electrical resistance model because it calculates one resistance for each control volume unlike the other models, which calculate only one resistance for two control volumes.

***Model 2D-1: Using Sammon's equation***

This model, already used by Hegre *et al.* (1986), uses the area plotted by a dashed line and the length *L* shown in Fig. A8. It is the scheme used in the commercial simulators that calculate the flux by two points.

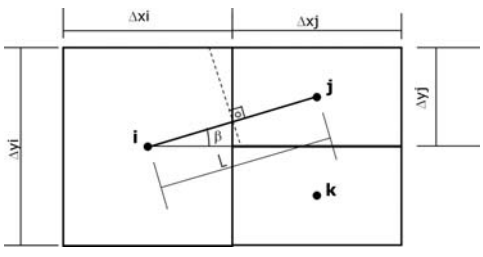


**Fig. A8 – Dimensions used in model 2D-1**

Both the lenght $L$ and the transversal area $A$, represented by the dashed line in Fig. A8, are given by

$$L = \left( \frac{\Delta x_i}{2} + \frac{\Delta x_j}{2} \right) \frac{1}{\cos \beta} \quad \text{and} \quad A = \frac{\Delta y_j}{\cos \beta} \tag{A11}$$

Supposing a uniformly spaced grid ($\Delta x_i = \Delta x_j$), the conductance expression yields

$$U_{ij} = k \cdot \frac{\Delta y_j}{\Delta x_i} \tag{A12}$$

For the volumes $j$ and $k$, the conductance is given by

$$U_{jk} = k \cdot \frac{\Delta x_j}{\Delta y_j} \cos^2 0^o = k \cdot \frac{\Delta x_j}{\Delta y_j} \tag{A13}$$

***Model 2D-2: Using the correction factor cos² β***

The angle $\beta$ is defined here as the angle formed between the line that joins the centers of neighbor volumes and the horizontal line, as shown in Fig. A9.

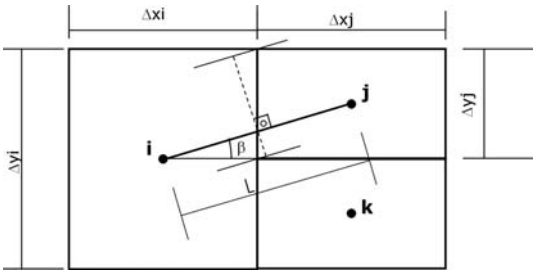


**Fig. A9 - Dimensions used in model 2D-2**

In this model, the length $L$ is the same of the model 2D-1, and the transversal area, represented by the dashed line in Fig. A9, is given by

$$A = \Delta y_j \cos \beta \tag{A14}$$

Due to the fact that the grid is uniformly spaced, we have $\Delta x_i = \Delta x_j$, and therefore the conductance between the volumes $i$ and $j$, $U_{ij}$, is given by

$$U_{ij} = k \cdot \frac{\Delta y_j}{\Delta x_i} \cos^2 \beta \tag{A15}$$

For the volumes $j$ and $k$, the conductance is the same of the Model 2D-1.

***Model 2D-3: Using Voronoi Grid***

In the Voronoi grid (Maliska, 1995), the transversal area used is located in the middle point of the cells' centre-to-centre line. For this grid, the conductance between the volumes $i$ and j is the same that was calculated by model 2D-1 since the areas utilized in these models are identical, as shown in Fig. A10. The construction is done in such a way that the line joining two grid-points is normal to the control volume's surface.

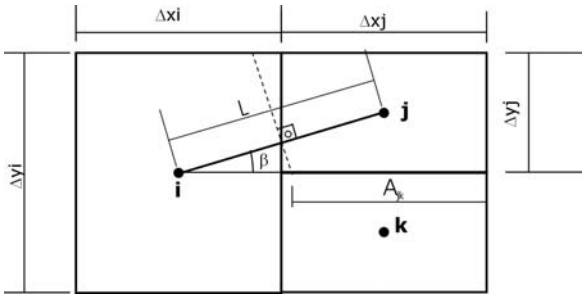


**Fig. A10 - Dimensions used in model 2D-3**

The only difference between this model and the model 2D-1 is the conductance between the $j$ and $k$, where the area utilized is $A_{jk}$ in Fig. A10, which is less than the area utilized in previous models, and is given by

$$A_{jk} = \Delta x_j \left( 1 - \frac{tg^2 \beta}{2} \right) \tag{A16}$$

Therefore, the conductance values for this case are

$$U_{ij} = k \cdot \frac{\Delta y_j}{\Delta x_i} \quad \text{and} \quad U_{jk} = k \cdot \frac{\Delta x_j}{\Delta y_j} \left( 1 - \frac{tg^2 \beta}{2} \right) \tag{A17}$$

The alteration of the area value between the volumes $j$ and $k$ resulted – at least in terms of connectivity – the change of the grid for the one shown in Fig. A11, which became a Voronoi grid. It is important to notice that the alteration of the normal flux surface for conductivities $U_{ij}$ and $U_{jk}$ identifies the two-dimensional characteristic of this problem.

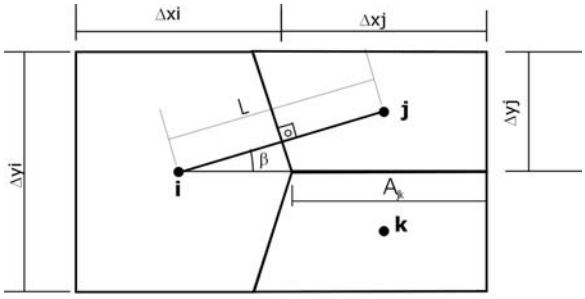


**Fig. A11 – Effective grid where are determined the conductances by Voronoi method**

### *Model 2D-4: Using the electrical resistance*

In this model the conductance between two volumes is calculated as the harmonic averaging weight of the conductances calculated for each neighbor. Note that this model is the same used for one-dimensional problem presented earlier (Model 1D-1), therefore we will not show the conductance expressions again.

### *Comparison between the models*

In the following sequence we present the results of the heat transfer problem defined in Fig. A6 for the four different models described here. The differences verified in the coarse and fine grids depicted in Fig. A7 are also shown.

In Fig. A12 are plotted the results for the volumes that are contained in the vertical line located in $x = 0{,}5$. It is compared the solution of four models in relation to the analytical solution. Note that the Voronoi model (Model 2D-3) showed the best solution, while the worst errors are found through the resistance model (Modelo 2D-4). Note also that the grid refinement did not contribute to increase the accuracy of the results.

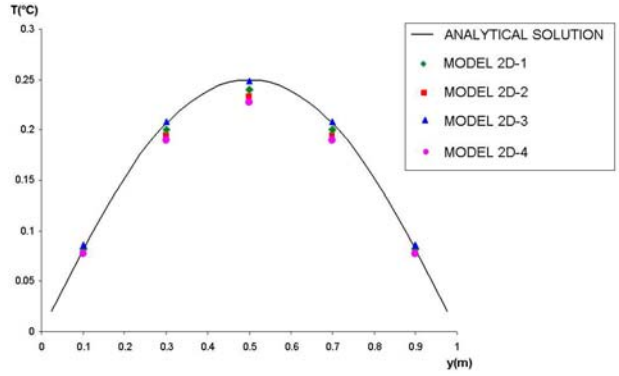


*(a)*

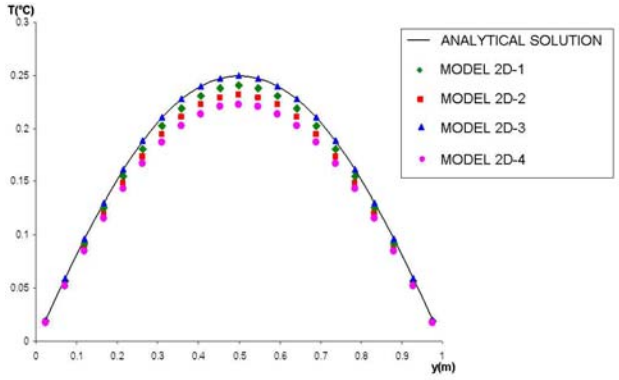


*(b)*

**Fig. A12 – Comparison between the temperatures obtained through different models and the analytical solution for *(a)* coarse and *(b)* fine gri**